Santosh_Thesis_KUS2

by Prabal Pratap Singh Bhadauria

Submission date: 07-Apr-2025 05:17PM (UTC+0530)
Submission ID: 2620002968
File name: Santosh_Thesis_KUS.docx (673.02K)
Word count: 26900
Character count: 143155

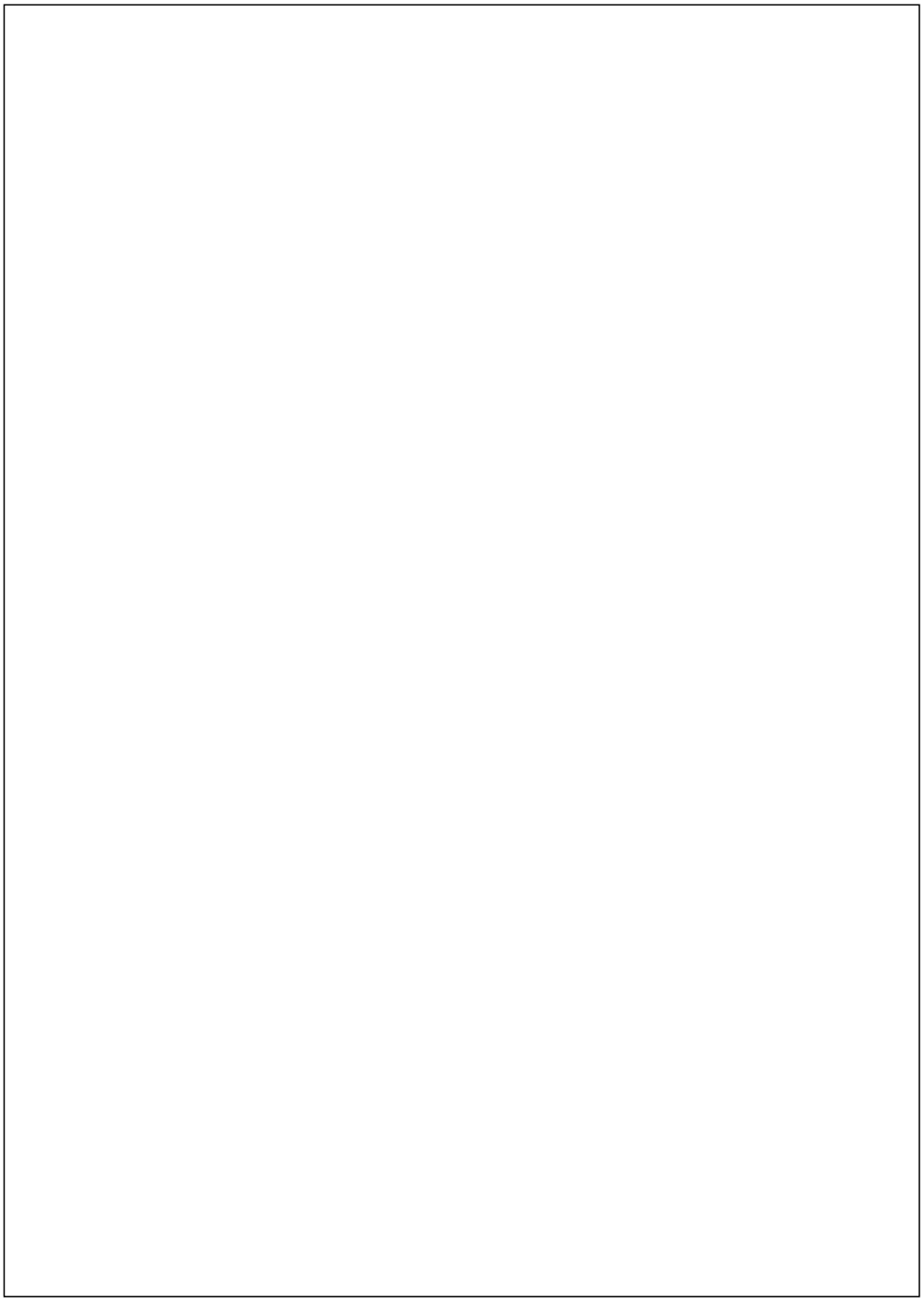

Chapter 1

Introduction

Overview

Glass is a very important component in automobiles. Two types of glass are used in automobiles: toughened (or tempered) and laminated glass. This chapter will discuss the basics of glass, followed by the required properties for windshield glass in vehicles, and how these properties are adapted for automotive applications. Furthermore, this chapter describes the types of glass used in automotive applications, their required properties, and the role of structural units and various components in silicate-based glasses used in automobiles.

1.1 Glasses for automobiles

Glass has a wide range of applications based on specific needs. There is a significant difference between the glass used in windows and that used in windshields of automobiles. A car's windshield is specially designed to withstand harsh conditions and also serves as structural support for the car's roof. Two types of glass are commonly used in automobiles:

(i) **Laminated glass (LG):** It consists of two sheets of glass bonded together with a layer of polyvinyl butyral (PVB) plastic at high temperatures [1] as shown in **Figure 1.1.** This type of glass has increased strength and provides support to sudden shatter after external impact [2]. Additionally, LG acts as a cushion for passengers who might be thrown against the windshield. It is used in the production of both front and rear windshields. When rocks or pebbles hit the windshield, only the outer layer is typically damaged, which can often be repaired without replacing the entire windshield glass/screen.

(ii) **Tempered glass (TG):** It is produced by heating curved glass to a high temperature followed by rapidly cooling. It is commonly used for the side windows of vehicles, as it is 10 times stronger than regular glass. Upon impact, it shatters into small, less harmful pieces, but cannot be repaired once broken [3]. Tempered glass is commonly used in applications such as furniture tops and the side and rear windows of automobiles [4]. Due to its strength and ability to withstand impacts and temperature variations this glass is also used for automotive sunroofs.

The TG are made with the presence of nitrogen and hydrogen gases, along with advanced oxygen-burner technology. In contrast, windshields that are made from laminated glass, where the presence of nitrogen gas between the two layers helps ensure that, if broken, the glass forms blunt, less dangerous pieces [5]. An interlayer material enhances mechanical properties such as impact strength and fracture toughness, while also altering the failure mode (fracture pattern) of LG [6]. The interlayer also helps to hold together broken pieces, reducing the risk to the life of the human being [1]. The influence of the interlayer material on the stiffness, impact strength, fracture pattern, and load-bearing capacity of LG is well-documented in applications like windshields, photovoltaic panels, and structural glass [7].

PVB and cross-linked ethylene vinyl acetate (EVA) are the most commonly used interlayer materials for laminated glasses. LG absorb impact energy and enhances brittle fracture performance compared to regular glass [8]. This advantage encourages designers to use LG in areas with a high risk of injury from glass breakage. Additionally, lamination can block ultraviolet radiation, especially when cerium is added as an adhesive, and also helps reduce noise [10, 23]. As a result, LG is widely used in automotive and structural applications. Curved structures, such as those found in automobile glass, offer greater resistance to external forces compared to straight beams, making them particularly effective in these applications.

1.2 Windshield glass and its composition

The main constituents of windshield glasses are soda-lime silicate (SLS) [2, 107]. The accommodation of various additives in glass composition changes the properties of glasses such as optical, mechanical, chemical stability, transparency, non-linear refractive index, etc [12, 13, 25]. Furthermore, these properties are tuned accordingly to change various properties, modifiers amounts, and their chemical nature, as well as other parameters. Windshield glass is not a single compound, its chemical formula is a combination of alkali oxides, alkaline oxides, and silica dioxide, along with some intermediate oxides such as Al_2O_3, TiO_2 etc. The general chemical formula for glass can be written as aX_2O-bYO-$cSiO_2$, where

a, b and c represent the number of molecules, X is an alkali atom (Na, K), and Y is an alkaline atom (Ca, Mg). For instance, soda-lime glass has the formula Na_20-CaO-$Si0_2$, while potash-lead glass is expressed as K_20-PbO-$Si0_2$.

1.3 Essential properties of windshield glass

Windshield glass in automotive applications must meet stringent safety, performance, and durability standards. The essential requirements for windshields suitable for automotive, as summarized from the previous discussion, include the following points:

- Windshields must resist minor impacts from debris, such as stones, without immediately cracking.
- The windshield must provide clear visibility for the driver. This includes minimal distortion, especially when looking through curved areas of the glass.
- The windshield must bond strongly with the car's frame to maintain its structural role, particularly during accidents or in case of airbag deployment.
- Automotive windshields are exposed to variable temperatures. The glass must endure both high and low temperatures without cracking or losing its integrity.

Overall, key factors such as strength, thermal expansion coefficient, optical transparency, and manufacturability are crucial when assessing the suitability of a material for use as windshield glass in automotive applications. **Table 1.1** outlines the engineering requirements for windshield glass in automotive applications. These parameters emphasize the superior safety of laminated glass compared to tempered glass, particularly in car accidents and, more specifically, in preventing passenger ejection during rollovers. Laminated glass is also superior in terms of security due to its higher resistance to fracture. The composition of soda-lime silicate glass for automotive applications has been optimized in such a way as to achieve the requirements as mentioned in **Table 1.1**.

1.4 Structure of silicate glasses

Continuous three-dimensional networks form in these glasses through the corner-sharing of these tetrahedral structures, further satisfying Zachariasen's criterion. The structural disorder is caused by variations in the bond angles of Si-O-Si linkages between neighbouring tetrahedral units. This results from the rotation of adjacent tetrahedra connected at their corners by oxygen atoms and the rotation of the oxygen atoms aligned with the silicon atoms. **Figure 1.2** provides a schematic represen- tation of these rotations in vitreous silica. Diffraction studies, aligned with the crystalline structure of Si-O tetrahedra, reveal that the shortest Si-O bond length is approximately 1.61 Å, while the O-O bond length is about 2.63 Å [16]. Despite the disordered arrangement of tetrahedra in the vitreous state of silicates, the variations are minimal due to the high degree of order within the fundamental tetrahedral units. The distance between two silicon atoms, measured from the centre of linked SiO_4 tetrahedra, is around 3.12 Å, causing variability

in the Si-O-Si bond angles. This distribution widens further for silicon to second oxygen (~4.14 Å) and oxygen to second oxygen (~5.1 Å) pairs [2,17].

1.4.1 Different structural units in silicate glasses

Therefore, as corner connectivity increases, the NBO/T ratio decreases. Additionally, as corner connectivity increases, the number of free oxygen atoms also rises.

This concept can be explained using the simple reaction presented in **equation 1.3** below:

$$SiO_4^{4-} + SiO_4^{4-} \rightleftharpoons Si_2O_7^{6-} + O^{2-} \quad (1.1)$$

The basic description provided above of vitreous silicate is sufficient for understanding the structure of any silicate-based glass.

1.4.2 Role of alkali and alkaline in silicate glasses

The understanding of glass structure has been significantly enhanced by the development of X-ray diffraction (XRD) techniques. Initial studies demonstrated that the structural unit in crystalline SiO_2 is a tetrahedron, with a Si^{4+} ion at the centre and an O^{2-} ion at each of the four corners, as depicted in **Figure 1.3 (a)** [20]. For charge neutrality, each oxygen ion must bond to two silicon ions, allowing the O^{2-} ion to be shared by two neighbouring tetrahedra. In crystalline structures, these units are organized in a regular

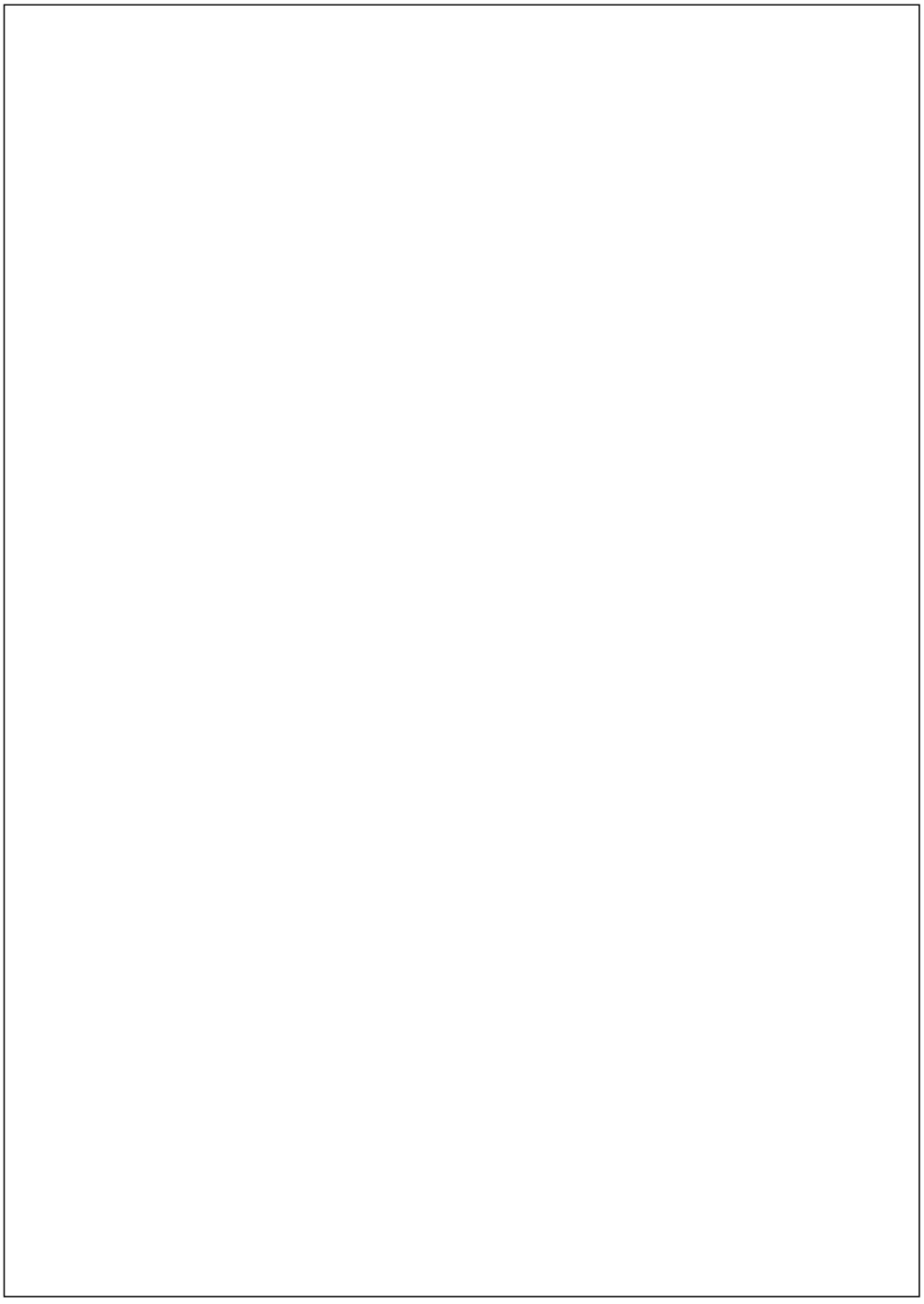

three-dimensional pattern, while in glass, they are randomly arranged. In **Figure 1.5 (a)**, the structural units are shown in a periodic arrangement typical of crystalline quartz, while **Figure 1.5 (b)** represents the non-periodic, disordered arrangement of these units in the glass. When modifying oxides like alkali (Li_20, Na_20 and K_20) and alkaline (MgO and CaO) are added to silica, the O to Si ion ratio increases. These additional ions disrupt the glass network, breaking its continuity at the points where they are introduced. As a result, the network becomes less rigid as shown in **Figure 1.6**. Alkali (Li^+, Na^+, and K^+) and alkaline (Mg^{2+} and Ca^{2+}) ions settle into the spaces formed by the network disruption. Due to their smaller size, Na ions can move between these spaces with relatively low energy, allowing them to maintain some mobility even at room temperature [21]. This significantly impacts various glass properties, such as optical, thermal, and mechanical properties [2,17].

1.5 Role of structural units in windshield glass

Furthermore, the abil-

ity to modify the various properties of glass like refractive index, hardness, and density through variations in composition suggests that the material can be feasible for automotive applications.

(i) **Mechanical properties:** The mechanical strength of silicate glass is directly related to the connectivity of the silicate network, represented by In a highly connected network (e.g., Q^4 units, via bridging oxygens), the glass tends to be more rigid and resistant to defor- mation [22]. A higher proportion of bridging oxygens (BOs) between silicate units increases the network connectivity, providing greater structural integrity [23]. This results in stronger, more durable glass, which is essential for automotive applications like windshields, where high strength is necessary to withstand impacts from debris and other stresses. A glass net- work with more NBOs (associated with Q^1 and Q^2 units) tends to be less rigid but

more flexible, which can improve the material's ability to absorb impact energy without shattering [58]. The mechanical performance of silicate glass under stress is highly dependent on how its network structure responds to force. A more open structure, with more NBOs (found in Q^2 or Q^1 units), may introduce points of weakness where fractures can initiate. However, in some cases, these structural features can allow for controlled fracturing, which is important for safety glass (e.g., tempered or laminated glass) used in automotive applications. The degree of network connectivity in silicate glass influences its resistance to surface scratches and wear. A more densely packed silicate network (with higher Q^4 content) leads to greater hardness and, consequently, better scratch resistance [3,107]. Since hardness represents the strength of the bonds in a material and it is frequently correlated with cation field strength (CFS) in the case of mixed modified glasses [26]. The CFS of different constituents in glass plays a crucial role in modifying or forming the glass network [27]. For example, K^+ having a larger cationic radius than Mg^{2+}, which has a lower attraction, corresponds to the weakest field strength from the oxygen that is not bridging [26]. While K^+ generates more of its coordinate linkages, it does not appropriately strengthen the structure because of its connection with NBOs.

(ii) **Thermal properties:** In manufacturing of windshield glasses, it is necessary to sandwich a polymer layer so that it can bear maximum load as well and during accidents, glass would not be shattered easily [107]. Thus, the fibre drawing is a reheating process that requires very high temperatures, it is ideal for a glass host to have as much space as possible to establish a wide working range of temperatures while manufacturing windshield glasses. The literature has observed that glass can be regarded as thermally stable if the value of ΔT is greater than 100°C [14, 108]. The structural rigidity of silicate units also impacts the thermal stability of the glass, which is important for applications like automotive windshields that undergo frequent temperature changes. Glasses with higher connectivity (Q^4) are more thermally stable and exhibit lower thermal expansion, ensuring they maintain their shape and optical properties under heat.

The thermal expansion of silicate-based glasses is governed by the asymmetry in thermal vibration amplitudes within the glass. As the rigidity of the glass network increases, thermal expansion decreases. An increase in non-bridging bonds weakens the

structure, leading to a higher coefficient of thermal expansion (CTE). Changes in the coordination number of network-forming cations can either increase or decrease the expansion, depending on their effect on the glass structure [30]. The CTE of commonly available soda-lime glass is typically > 10×10^{-6} K^{-1}, but it can be adjusted by altering the glass composition [108]. Alkali and alkaline earth metal oxides significantly influence the CTE of silicate-based glasses. Alkali and alkaline earth metal oxides act as network modifiers, breaking the Si-O-Si bonds within the silica network and generating NBOs. This disruption weakens the glass network and reduces its rigidity, resulting in higher CTE values due to increased thermal expansion susceptibility.

(iii) **Optical Properties:** Windshield glass typically has a visible light transmittance of approximately 70%, allowing sufficient light to pass through for clear vision while driving [31]. Most regulations require windshields to transmit at least 70-75% of visible light [32]. Modern windshield glass often includes a coating or laminate that blocks a significant portion of UV rays, preventing harmful radiation from entering the vehicle. UV transmittance is kept very low to protect passengers and reduce interior fading. These optical properties balance safety, comfort, and visibility for drivers and passengers. The arrangement and connectivity of silicate structural units (Q^n units) influence the transparency of the glass. A highly connected glass network (Q^4) offers better structural rigidity and optical clarity, which is essential for automotive windshields and windows to ensure visibility and safety [33]. Fewer NBOs result in reduced scattering of light, thus enhancing transparency [3]. Silicate glass can be optimised for UV protection by modifying the network structure with additives such as iron or titanium. This is important for automotive windows, where UV protection is needed to prevent interior fading and protect passengers from harmful rays [34]. Modifications in the silicate network reduce the number of non-bridging oxygens, influencing UV absorption characteristics. The presence of alkali/alkaline modifiers within the silicate structure can change the arrangement of the Q^n units, increasing the refractive index, which is useful for headlamps.

In automotive applications, the mechanical properties of silicate glass, such as strength, toughness, thermal expansion resistance, and scratch resistance, are strongly influenced by the arrangement of silicate structural units. High network connectivity (more Q^4 units)

leads to stronger, more rigid glass with better scratch and chemical resistance, while lower connectivity (more NBOs) can improve toughness and flexibility. By carefully tailoring the silicate structure, manufacturers can optimize the mechanical performance of glass for specific automotive requirements, balancing impact resistance, durability, and thermal stability.

1.6 Windshield glass and recycling

Globally, carbon reduction is a primary concern in environmental protection efforts. However, the treatment and recycling of glass present significant challenges, often proving to be difficult, costly, and impractical. A viable approach to address this issue involves the dismantling of glass from End-of-Life Vehicles (ELVs), followed by its collection, transportation to treatment facilities, purification, and subsequent conversion into reusable, clean raw glass, commonly referred to as cullet [35]. Cullet represents a valuable resource that can be reintroduced into glass production processes, effectively substituting for virgin raw materials. The utilization of cullet offers two primary advantages to the glass production industry: it is typically more cost-effective than sourcing raw materials such as silica, and it requires less electrical energy during the re-melting process in furnaces [36]. Furthermore, the reuse of cullets contributes to the conservation of natural resources by minimizing the need for their extraction, transportation, treatment, and consumption in the production of new glass products [37]. Consequently, the adoption of cullet reuse initiatives provides a positive and multifaceted contribution to environmental conservation. Moreover, the recycling of oxide glasses does not result in the evolution of CO_2 during the recycling process. Thus, recycling not only reduces carbon footprint, costs, and processing time but also conserves raw materials. The central theme of this research work is to explore the recycling of waste windshield glass for automotive applications. Therefore, conducting "studies on the optical, thermal, and mechanical properties of glasses for automotive applications" alongside policies promoting reduction, recycling, and reuse, represent effective strategies for minimizing the carbon footprint within the glass industry.

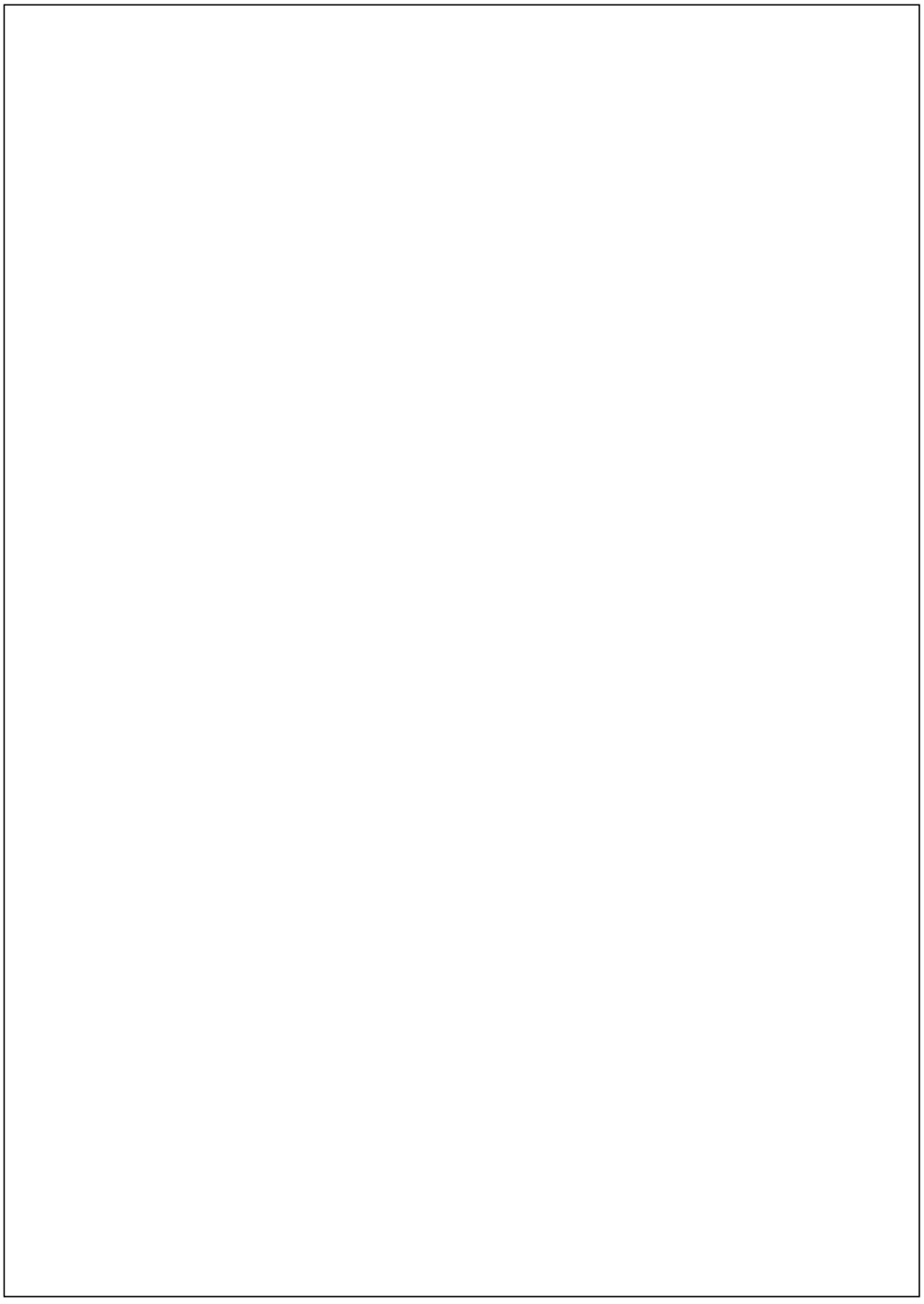

Chapter 2

Literature review

Overview

This chapter presents a comprehensive review of the literature on silicate-containing alkali and alkaline earth oxide glasses for automotive applications, particularly windshield glasses, which highlights their critical role in enhancing the mechanical, thermal, and optical properties of automotive glasses. Alkali, alkaline, and intermediate oxides influence the optical properties of the glasses, such as transparency and refractive index along with other properties. The presence of these oxides usually reduces the melting temperature and allows for high optical clarity, which is critical for vehicle windshields and windows. Based on this literature review, the motivation of the present study along with the objectives of the thesis are outlined at the end of this chapter.

2.1 Role of modifiers in silicate glasses

Si–O–Si bonds. This process transforms some bridging oxygens within the fully interconnected SiO_4 tetrahedral network into non-bridging oxygens singly bonded to silicon. This disruption also leads to a decrease in viscosity, facilitating glass processing at lower temperatures.

2.1.1 Alklai oxides

Alkali oxides (Li_20, Na_20, and K_20) are gaining interest due to the functionalised and modified properties of glasses, with a focus on user needs with reducing development costs [1]., leading to the formation of NBOs as shown in **Figure 2.1**. This disruption decreases the network's rigidity, thereby influencing various glass properties. The concentration of NBOs directly affects the glass's optical properties, including the optical band gap as well as the refractive index.

Several studies have focused on the so-called "mixed alkali effect" (MAE), observed when two or more alkali oxides are present in a glass matrix. The modification of silicate glass networks through the substitution of one alkali oxide in place of another has been the subject of considerable research due to its profound impact on the resulting material properties. A seminal study by Grund et al. [6] investigated the $(20-x)Na_2O-(x)K_2O-10CaO-70SiO_2$ system, demonstrating that the substitution of Na_2O with K_2O leads to an increase in density and a concomitant decrease in molar volume. This system exhibited characteristics of the MAE, including a maximum in microhardness and a minimum in the T_g, accompanied by an increased atomic packing density at intermediate compositions. Based on Raman spectroscopy analysis, it was observed that the higher field strength of Na^+ (0.96 $Å^2$) ions tend to displace the lower field strength K^+ (0.52 $Å^2$) ions to lower energy sites, significantly This finding highlights the crucial role of ionic field strength of modifiers in determining the change in local structural units of alkali-modified glasses. Building upon this understanding of alkali ion interactions, characteristics were reported that Young's modulus de- creases with increasing K_20 concentration, indicating a reduction in mechanical stiffness. of K_20 compared to Na_20 [8]. Furthermore, Shen et al. observed an increase in the coefficient of thermal expansion (CTE) with the incorporation of K_20, which eventually stabilised at K_20 concentrations exceeding 3.9 mol%. This stabilisation suggests a satura- tion effect on the thermal expansion characteristics, where additional K_20 beyond this point does not further enhance thermal expansion. These studies demonstrate that substituting one alkali oxide with other impacts mechanical and thermal properties through structural alterations within the glass network. The effects of Li_20 as a network modifier have also received significant attention. Gaurav et al. [9] explored the role of Li_20 in modifying the Si-O network through interactions with non-bridging oxygen (NBO) atoms. The addition of Li_20 led to alterations in properties such as molar volume and interionic distances, which were observed to exhibit a random trend. The incorporation of Li_20 also resulted in a decrease in the optical bandgap (E_g) and the Urbach tail (E_u), accompanied by an increase in the refractive index (n). These changes were attributed to an increase in structural disorder

induced by Li_20 incorporation, suggesting a structural modification mechanism different from that of K_20 substitution. Furthermore, the influence of Li_20 on other silicate systems has been investigated in the system $(x)Li_2O - (85 - x)Bi_2O_3 - 15SiO_2$ [10]. These researchers observed a reduction in the strength of the glass network, manifested as a decrease in T_g with increasing Li_20 content, consistent with the breaking of bonds in the glass network. A progressive shift of the absorption edge toward longer wavelengths was also observed with increased Li_20, which is indicative of NBO formation. These findings corroborate that alkali ions interact with the network differently depending on their specific ionic properties, demonstrating that the overall modification of silicate glass by alkali ions is a complex process. This complexity is reflected in the variations observed in E_g, which are understood to result from structural changes induced by the progressive addition of Li_20. Complementing experimental investigations, computational approaches have proven invaluable in understanding the structure-property relationships within silicate glasses. Molecular dynamics (MD) simulations, often coupled with techniques like Brillouin light scattering (BLS) spectroscopy, have been extensivelyutilisedd to probe the structural and mechanical attributes of sodium silicate glasses as a function of Na_20 content [11, 12]. These studies have revealed nuanced relationships between composition, network structure, and mechanical behaviour. At low Na_20 concentrations, simulations indicate the formation of clusters which diminsh the overall attractive interactions within the glass network. This decrease in compactness is attributed to the low content of Na_20 which leads to the generation of free volume within the network, ultimately contributing to lower elastic constants and a generally "softer" glass structure. Conversely, at higher Na_20 contents ($x \geq 20\%$), a marked increase in network cohesion was observed [12]. This enhanced cohesion results from the forming of Na-O and Si-O bonds coupled with a more homogenous distribution of sodium oxide within the structure. This structural reorganisation consequently enhances the mechanical strength of the glass. These simulation results underscore the sensitivity of silicate glass properties to the distribution and concentration of network-modifying alkali oxides. To further understand the effects of Na_20 incorporation, Baral et al. [13] employed Ab Initio Molecular Dynamics (AIMD) to construct sodium silicate glass models with varying Na_20 concentrations. Their simulations provide a deeper atomistic perspective on structural modifications by demonstrating that the bond order density (BOD) decreases with increasing Na_20. This reduction in BOD reflects the progressive disruption of the silica

network connectivity as BOs are converted into NBOs. These structural changes are accompanied by concomitant alterations in bond lengths and angle distributions, ultimately affecting the bulk properties of the material. As Na_2O content increased, Baral et al. observed an increase in both density and refractive index, while the BOD and optical bandgap were shown to decrease. Their calculations also indicated a decrease in elastic properties, specifically Young's and shear moduli. Notably, the bulk modulus showed a non-monotonic trend with increasing Na_2O content, reflecting the competing effects of network disruption and increased atomic packing. These findings are particularly valuable, as they explain the complex nature of how varying network modifier concentrations and the resultant alteration of the network structure can have a different effect on the elastic properties. Furthermore, the simulations suggested an increase in Poisson's ratio at higher Na_2O concentrations, indicating enhanced ductility, although the structural network was found to become less stable above 40 mol% of Na_2O due to extensive disruption. This comprehensive investigation into the atomistic structural modifications as a function of Na_2O content provides critical insights into how alkali oxide inclusion can alter the mechanical properties of the silicate gasses.

2.1.2 Alkaline earth oxides

Alkaline-earth metal ions, function as network modifiers within the silicate glass structure. Their introduction disrupts the continuity of the three-dimensional silicon-oxygen network, lead- ing to significant alterations in resulting glass. This structural modification is achieved through the interaction of the divalent alkaline-earth cations with non-bridging oxygen (NBO) atoms, which are created when Si-O-Si linkages are broken. affects numerous macroscopic characteristics. CaO andMgO-basedd silicate glass systems have emerged as materials of significant interest within the non-metallic materials sector, owing to their attractive physical and chemical properties, including excellent thermal stability and superior optical transmission [14]. The combination of these characteristics renders $CaO-MgO-SiO_2$ glass systems highly promising for diverse industrial applications [15,16]. The glass composition $5SiO_2$-$10K_2O$-(35-x)CaO-(x)M gO was synthesised using the melt-

quenching technique, and its structural and optical properties were comprehensively studied [17]. It is observed that glasses containing higher MgO levels exhibited better polymerisation and a more compact glass network compared to those with higher CaO content, attributed However, the Urbach energy values showed no consistent trend with the replacement of CaO by MgO, likely due to the similar chemical characteristics of both the oxides. This study highlights the critical role of compositional variations, particularly the substitution of CaO with MgO, in tailoring the The influence of alkaline-earth metal oxides on silicate glass properties exhibits a concentration-dependent effect. Varia- tions in the concentration of a single alkaline-earth oxide or more complex mixtures of two or more result in a non-linear change of the glass's properties. Specifically, the non-linear behaviour when multiple alkaline-earth metal oxides are introduced is termed the mixed alkaline-earth effect (MAEE). The presence of multiple alkaline-earth cations introduces complex structural environments that affect the transport and reactivity of the silicate network. Conversely, bulk properties, such as density, the CTE, and refractive index, tend to be less sensitive to the mixed alkaline-earth composition (MgO-CaO), exhibiting smaller deviations from linearity [18].

A number of studies have explored the influence of the MAEE on the properties of silicate-based glasses. One such investigation focused on Al_2O_3−SiO_2 glasses, examining the impact of MAEE on Vickers hardness, brittleness index, and characteristic glass temperatures [19]. The study revealed notable differences in the structural influence of Mg^{2+} and Ca^{2+}ions. Specifically, due to the shorter and stronger Mg-O bond, MgO-containing glasses exhibited a decreased atomic density when compared to their CaO-containing counterparts. This higher field strength of Mg^{2+} is associated with a deeper potential energy well, which, in turn, diminishes the anharmonic vibrations at a given temperature, resulting in a decrease of the CTE [20]. Conflicting results have been reported concerning the influence of alkaline

earth substitution on the T_g. It has been observed that the higher bond strength between Mg and oxygen (O) compensates for the smaller coordination number of Mg^{2+}, leading to an increase in T_g [21]. However, Kjeldsen et al. [19] observed temperature (T_g) with the substitution of MgO, attributing this decrease to potential bond weakening in the local structural environment surrounding the network modifiers. These contrasting findings underscore the complex interplay between the network structure and the mobility of the constituent ions in these glasses. Interestingly, despite the observed varia- tions in hardness, brittleness, and characteristic temperatures, some studies have found that the elastic moduli of these glasses remain largely compositionally invariant [19, 22]. This suggests that the variations observed in microhardness and shear viscosity are closely asso- ciated with the translational motion of structural units rather than changes in the inherent stiffness of the glass network. It indicates that the same underlying topological constraints govern both microhardness and shear viscosity, and compositional variations may not significantly alter the onset of rigid T_g constraints. This highlights that the dynamic response of the network is more sensitive to the mixed alkaline earth effect than the overall stiffness of the materials.

The incorporation of MgO and CaO as network modifiers has been shown to significantly alter the structure and, consequently, enhance the mechanical properties of silicate glasses [23, 24]. In the $25RO - 20Al_2O_3 - 55B_2O_3$ glass system (R = Mg, Ca, Sr, Ba), the T_g increases from 554 to 636°C. The higher field strength of alkaline-earth modifiers contributes to increased hardness and T_g which is attributed to the formation of stronger bonds between the modifiers and NBOs [97]. This investigation highlights the importance of chemical composition tuning in achieving the desired balance of mechanical properties in $Al_2O_3 - B_2O_3$ glasses, paving the way for their use in advanced engineering applications. In the sodium borosilicate glass system $9.4Na_2O - 25.4B_2O_3 - 65.2SiO_2 - (x)CaO$ (where x = 0 to 15), calcium acts as an intermediate oxide [26]. For Ca < 3.3%, calcium acts similarly to sodium. For Ca > 3.3%, the formation of Si-O-CaO-B/Si-O-CaO-Si units occurs, leading to the saturation of four-coordinated boron units i.e., BO_4. These findings provide a deeper understanding of CaO, which plays a dual role in glass systems, offering insights into tailoring properties for specific applications. A pronounced mixed alkaline-earth effect was observed, characterised by a negative non-monotonic deviation in Vicker's hardness (H_d) as Sr was substituted for Cain above glass composition. This deviation indicates a complex interplay

of network-modifying roles of alkaline-earth elements in the silicate series [27]. In contrast, the aluminate series exhibited a near-linear compositional dependence of H_d, with weaker mixed alkaline-earth effects. This difference is attributed to the charge-balancing role of alkaline-earth ions in aluminates as opposed to their network-modifying role in silicates. The contrasting behaviour of silicate and aluminate systems highlights the distinct structural roles played by alkaline-earth ions. In silicates, alkaline-earth elements act primarily as network modifiers, introducing NBOs and disrupting the glass network. In aluminates, these materials serve as charge-balancing agents for the alumina tetrahedra, contributing to the stability and rigidity of the network. These roles significantly influence macroscopic properties such as hardness, viscosity, and CTE.

The combined impact has also been investigated. A study by Hu et al. [34] demonstrated that substituting both CaO and MgO in a $Li_20 - Al_2O_3$ leads to a decrease in the crystallisation temperature, a shift in the crystallisation mechanism from bulk to surface crystallisation, and an increase in both
flexural strength and fracture toughness. These findings highlight the complementary interaction between CaO and MgO in effectively tailoring the thermal and mechanical properties

of silicate glasses. Furthermore, Kjeldsen et al. [19] found evidence that the MAEE affects T-O-T bonds (where T represents a tetrahedral unit) and, interestingly, indicated that the network connectivity of mixed CaO-MgO compositions is higher compared to glasses with a single alkaline earth modifier in similar glass composition. This observation highlights the complex structural changes induced by the mixing of different alkaline earth ions within the silicate network. These results suggest that the MAEE influences the structural arrangement, potentially by favouring different types of bonding arrangements and network topologies that do not directly translate to changes in overall stiffness as reflected by the elastic modulus. In contrast to this, other investigations have explored the relationship between and the elastic modulus of silicate glasses. Based on these results, Kacper Januchta et al. further proposed a linear Their work indicates a di- rect correlation between the ionic field strength of the modifying cation and the mechanical properties, which contradicts Kjeldsen's findings that the elastic modulus is unaffected by the MAEE. These findings reveal that the impact of the MAEE on the mechanical proper- ties of silicate glasses is complex and multifaceted. While some studies suggest the elastic modulus is relatively insensitive to the mixed alkaline earth composition, others emphasise the direct effect of the modifier's field strength on various properties.

2.1.3 Alkali and alkaline earth oxides

Alkali and alkaline earth oxides are essential in glass formulations for automotive applications due to their combined effects on melting behaviour during processing, strength, durability, and optical properties. Structurally, it has been shown through both experimental methods and MD fine structure (EXAFS) confirm that these cations are primarily bonded not only to NBO ions but also to BO ions [38]. In silicate glasses, Q^n units define silicate tetrahedra with n BOs and (4-n) NBOs. The distribution of Q^n units depends on the field strength of the

modifier cation. For instance, in disilicate glasses, the proportion of Q^3 species rises as the cation's field strength decreases. While Q^2 and Q^4 units become more abundant with higher field strength cations [39,40]. Neuville's research on silicate glasses with mixed Na_20 and CaO revealed a similar trend in the Q^n distribution Examining the effects of modifiers such as Na_20, K_20, MgO, and CaO within a SiO_2 matrix is valuable [42]. Among these modifiers, Na_20 and K_20 consistently act as a glass modifier, generating a greater number of NBOs as compared to MgO and CaO.

It has been reported that substituting MgO and CaO instead of Na_20 leads to a decrease in compressive stress [44]. Bäck et al. [6] studied the physical The MAE is characterised by non-linear property trends, driven by the distinct interactions between high (Na^+) and low (K^+) field strength ions, as well as deviations in packing density. physical properties, such as density, molar volume, T_g and microhardness. With increasing substitution of BaO for CaO, density and molar volume increase while T_g as well as hardness decreases. The additive behaviour suggests weaker interactions between Ca^{2+} and Ba^{2+} resulting in linear property variations of the glasses. It is concluded that the mixed alkali and mixed alkaline earth systems exhibit contrasting behaviour. Seo et al. [45] observed that the transmittance of the glasses decreased as the alkaline/K_20 ratio increased in the $ZnO - B_2O_3 - SiO_2 - Al_2O_3 - RO - K_20$ system. This trend is attributed to structural densification and possible light scattering caused by increased alkali content.

The non-additive trends in the glass properties, including hardness and indentation toughness has been observed in the sodium-calcium aluminosilicate (NCAS) glasses having composition $(Na_2O)_{30-x}(CaO)_x(Al_2O_3)_{10}(SiO_2)_{30-x}$ [46]. The NCAS glass series exhibited a distinct MME in hardness and wear resistance. Glasses with intermediate ratios of alkali (Na_20) to alkaline (CaO) demonstrated superior resistance to wear, particularly under high humidity conditions. Despite these variations in mechanical properties, molecular dynamics

simulations suggested no significant trend in the network structure with composition. The structural dynamics of NCAS glasses, as investigated through density and bond angle distributions, deviated from trends observed in simpler silica glasses. The presence of multiple modifiers introduced increased structural freedom, which likely contributed to the observed nonlinearity in mechanical behaviour.

Alkali and alkaline-earth elements, when acting as network modifiers, significantly influence the glass formation, structure, and properties of glasses, especially when two types of alkali and alkaline-earth oxides are combined. The CaO-MgO and CaO-Li_20 mixed silicate glasses have been investigated, and it is observed a direct correlation between the volume of plastic flow and H_d [19]. The substitution of MgO with Na_20 in $Si0_2$ based glasses not only enhanced the mechanical properties of the glass but also altered its structural, optical, and thermal characteristics [47]. This glass system exhibits strong correlations between structural modifications and its macroscopic properties, paving the way for its use in applications such as transparent materials. The optical band gap increases with the substitution of Na_20 in place of MgO and it is attributed to the enhanced polymerization of the silicate network, as Na^+ ions scavenged metal cations and reinforced the bonding mechanisms. Young's modulus increased slightly from 80.891 to 82 GPa, correlating with the increased molar mass of the glass system, while Poisson's ratio exhibited a decreasing trend with increasing Na_20 content in place MgO. Vickers microhardness measurements demonstrated a noticeable improvement in the mechanical strength of the glass samples, further emphasizing the impact of these compositional modifications.

2.2 Role of intermediate oxides

Intermediate oxides in silicate glasses are those can act as former or modifiers. Thus, intermediate oxides Unlike network formers (such as $Si0_2$ and B_2O_3), which establish the fundamental framework of the glass structure, or which disrupt the network by creating NBOs, intermediate oxides exhibit a more versatile behaviour. These oxides can act as either network formers or modifiers, depending on the specific composition, local structure, and bonding environment within the

glass. Common intermediate oxides encountered in silicate glasses include Al_2O_3, TiO_2, and ZrO_2 [48]. Their incorporation can dramatically alter mechanical, optical, and thermal properties, making them critical components in the design of functional glasses.

This improvement is attributed to the high field strength of Zr^{4+} ions instead of Ba^{2+}, which promote the formation of more rigid structural units within the glass network, consequently enhancing stability and durability of the glass. However, the glass stability criterion (T_g-T_c)

initially increased with ZrO_2 additions, maximise at 2 mol% of ZrO_2, and subsequently decreased with higher concentrations of ZrO_2. This observation suggests a change in the role of ZrO_2 within the glass structure, acting as a network former at lower concentrations but it act as a network modifier at higher concentrations of ZrO_2. This behaviour underscores the complex interplay of compositional factors in glass systems.

The inclusion of TiO_2 in the investigated system is noteworthy as TiO_2 is frequently employed as a nucleating agent in glass This property is crucial for producing glass-ceramics, but in the present context, it must be considered within the overall property profile. The study also noted that the addition of ZrO_2 This highlights a common trade-off in glass design, where the inclusion of certain components beneficial for one property may negatively affect others.

The modification of glass compositions through the incorporation of various additives has long been a subject of extensive research, aimed at tailoring specific properties for diverse applications. Among these additives, Al_2O_3 stands out due to its moderate strength, good thermal conductivity, and cost-effectiveness, making it a popular choice in glass formulations [52]. The addition of Al_2O_3 is particularly beneficial in enhancing the chemical durability, melting characteristics, and opacity of glasses [53], thereby expanding their suitability for optical and other demanding applications. Studies have consistently shown that Al_2O_3 plays a critical role in improving the mechanical properties of glasses. Mohamad et al. [54], for instance, investigated the impact of adding 2 wt% Al_2O_3 to a silicate glass system $(45SiO_2 - 24.5CaCO_3 - (24.5 - x)Na_2O - 6P_2O_5 - (x)Al_2O_3)$. Their findings demonstrated significant improvements in mechanical performance and sintering behaviour at elevated temperatures. This study provides further evidence supporting the notion that Al_2O_3 can effectively enhance the mechanical strength of glasses [54]. This enhancement is largely attributed to the replacement of Na_2O with Al_2O_3 within the glass network, resulting in a stronger covalent Al-O bond compared to the relatively weaker Na-O bond. The higher electronegativity of Al^{3+} compared to Na^+ is responsible for this increased bond strength. Beyond mechanical improvements, the inclusion of Al_2O_3 is also recognized for its ability to enhance chemical durability and reduce the CTE in glasses [55]. These benefits are essential for applications where thermal stability and resistance to chemical attack

are paramount. Furthermore, the presence of Al_2O_3 has been demonstrated to delay the devitrification process in glasses. This is crucial for maintaining the desired amorphous structure and preventing the formation of crystalline phases that can compromise optical and mechanical properties.

The silicate glasses, especially aluminosilicate glasses, exhibit properties suitable for various commercial applications, their high melting points present challenges for processing and manufacturing, leading to increased costs. An alternative approach is the use of aluminoborate glasses where B_2O_3 and Al_2O_3 act as network formers. The addition of B_2O_3 is decreased the melting temperature and facilitating easier control during the forming process [56].

The literature highlights the multifaceted role of Al_2O_3 as a valuable additive in glass systems. Its incorporation leads to, chemical durabil- ity, thermal properties, and resistance to devitrification. This makes Al_2O_3 an attractive component for The work of Mohamad et al. and others [52–55] provides a foundation for understanding and utilizing the benefits of Al_2O_3 in glass engineering.

2.3 Effect of two glass formers (SiO_2 and B_2O_3)

Silica (SiO_2) and boron oxide (B_2O_3) are fundamental constituents of numerous glass systems, each playing distinct roles that critically influence the resulting material's properties. SiO_2 acts as a primary network former, establishing a rigid, three-dimensional glass structure that provides mechanical strength and thermal stability. Conversely, B_2O_3, while also capable of forming a network, is recognized for its ability to enhance the adaptability of the glass structure and lower its melting temperature. The combination of these two oxides, as frequently seen in borosilicate glasses, results in a desirable balance of durability, thermal

resistance, and processability, making them suitable for a wide range of applications including chemical-resistant containers, laboratory apparatus, and display panels [48, 60].

The synergistic effect of combining SiO_2 and B_2O_3 has been the subject of numerous studies aimed at understanding their complex interactions within the glass matrix and their influence on material properties. Efa et al. [61] investigated the impact of B_2O_3 on the physical, thermal, and mechanical characteristics of aluminosilicate glasses. Their findings, based on Fourier-transform infrared (FTIR) spectroscopy, revealed that the incorporation of B_2O_3 led to the formation of B-O-B and Si-O-B bonds, indicating its successful integration into the glass network. These structural modifications directly impacted the glass's thermal and crystallization behaviour. Specifically, the addition of B_2O_3 suppressed crystallization, promoting an amorphous phase and thus enhancing the thermal stability of the glass. However, Efa et al. [61] also observed that increasing B_2O_3 concentrations resulted in a reduction in density, Vickers microhardness, and compressive strength. This decline in mechanical properties was attributed to the induced amorphization of the glass, coupled with the increasing presence of BO_3 units. These units increase structural flexibility and fragility, and the associated increase in molar volume further contributed to the observed degradation in mechanical performance. In a related study, Lian et al. [62] explored how compositional variations in borosilicate glasses, particularly the B_2O_3 content, influenced structural modifications and, consequently, phase separation and mechanical stability. Their work highlighted the dual role of boron depending on the availability of free oxygen within the network. When sufficient free oxygen is available, often due to the presence of alkaline oxides, boron exists primarily in the BO_4 tetrahedral form, which promotes a compact and chemically stable glass network. However, when free oxygen becomes limited, boron transitions to the BO_3 trigonal form. This transition results in a more layered structure (**Figure 2.2**) that reduces the chemical stability of glass. Further analysis of the spectra revealed vibrational characteristics linked to Q^n units, demonstrating the cleavage of bridging oxygen bonds and the depolymerization of the glass network. Specifically, the researchers noted the transition of Q^4 units to Q^3 units with increasing B_2O_3 content, a process that promotes high-temperature phase separation.

These studies collectively highlight the complex interplay between SiO_2 and B_2O_3 within glass systems. The addition of B_2O_3 improves thermal stability and processability but may reduce mechanical strength, depending on its incorporation and overall composition. Careful

control of B_2O_3 content is essential to optimize borosilicate glass for specific applications. The studies by Efa and Lian, in particular, provide valuable insights into the structural modifications induced by B_2O_3 and their consequences for both the thermal and mechanical characteristics of borosilicate glasses [61, 62]. These findings will be further explored for structural, optical, thermal and mechanical properties with alkali-alkaline-containing borosilicate glasses.

Building upon the established importance of SiO_2 and B_2O_3 in glass networks, further research has focused on understanding the nuanced effects of their compositional ratios on resulting material properties. Specifically, the impact of replacing B_2O_3 with SiO_2 has drawn significant attention, with studies revealing complex, non-linear trends in crucial properties. Kashif et al. [63] directly investigated the influence of this substitution on the structural and physical properties of glass systems. Their findings indicated that both the density and the glass-forming ability of the studied samples exhibited a non-linear relationship with the systematic replacement of B_2O_3 by SiO_2. This non-linearity was attributed to alterations in the glass network structure, specifically involving shifts in the ratio of boron structural units (BO_4 to BO_3) and changes in the concentration of NBOs in the glasses. These structural changes further impacted the mechanical properties of the glasses: both fragility and Vickers hardness followed similar non-linear trends with replacement of B_2O_3 by SiO_2, reaching maximum values at 5 mol% B_2O_3. At this specific composition, cor-

responding to a B_2O_3/Al_2O_3 ratio of 1, the study suggested that conditions favoured leading to a denser and more robust glass network. Conversely, at lower B_2O_3 contents, fragility and hardness de- creased due to an increase in NBOs concentration. leading to decreased mechanical strength and a less robust structure. However, with a further increase in SiO_2 content, the study observed an improvement in these properties, which was hypothesized to arise from the enhanced con- nectivity of the glass network via the silica species. The observations from Kashif et al. [63] resonate with existing literature demonstrating the inverse relationship between microhard- ness and NBO concentration [64]. which terminate the network structure, has been repeatedly shown to correlate with lowered microhardness. This is crucial to understanding how compositional variations im- pact the integrity of the glass material. Further exploring the trends within these complex glass structures, other researchers have observed similar non-linear behaviours related to SiO_2/B_2O_3 ratios in modified glasses. For instance, Thombre et al. [65] examined lithium borosilicate glasses and found that oxygen packing density, interionic distance, and polaron radius decrease, while ionic concentration increases, The authors concluded that these properties change non-linearly as the glass for- mer shifts, while the modifier concentration remains constant. Smedskjaer et al. [66], using concluded that the addition of SiO_2 in place of B_2O_3 leads to an increased formation of NBOs on SiO_4 tetrahedral structural units, contributing to structural disruption under specific conditions. Similarly, Fattah et al. [67], studying cobalt oxide doped borosilicate glass, found that adding SiO_2 results in an increase in the optical band gap, alongside a reduction of the structural defects. This observation suggests that higher SiO_2 concentrations may lead to a more ordered structure These findings highlight the detailed balance between different network-forming and mod- ifying oxides. While pure silica networks exhibit considerable strength, Doremus's theory posits that the incorporation of modifiers in silicate glasses generally results in lower strength compared to pure crystalline SiO_2 [68]. Supporting this assertion, Gehlhoff and Thomas [69] studied the tensile strength, elastic modulus, and modulus of rupture (MOR) of sodium sil- icate glasses with various oxide additions. Their work showed that substituting B_2O_3 for

SiO_2 significantly enhanced both the elastic modulus and overall strength of the glass when compared to similar substitutions using Al_2O_3. This further underscores the specific advantages that B_2O_3 can impart to glass structures despite its more complex role. These studies highlight the critical impact that the relative proportions of SiO_2 and B_2O_3 have on the resulting structural, physical, and mechanical properties of glass systems. The non-linear trends observed in density, glass-forming ability, fragility, hardness, and other related properties, underscore the delicate balance that exists within borosilicate glasses. The key role of B_2O_3 in both forming BO_4 and BO_3 structural units and the associated changes in NBO concentrations, demonstrate how these different network formers and modifiers can lead to drastically different materials properties. These observations have significant implications for the optimization of glass compositions for mechanical, optical and thermal properties for automotive applications.

2.4 Effect of alkali, alkaline and intermediate oxides on windshield glass

Borosilicate glasses represent one of the most technologically significant glass systems due to their versatile properties and wide range of applications. Notably, alkali borosilicate glasses, such as Pyrex, have long been used for applications requiring exceptional thermal shock resistance, while alkaline earth borosilicate glasses serve as base materials in liquid crystal displays (LCDs). The unique characteristics of borosilicate glasses, particularly in comparison to other glass systems, stem from the complex interplay between SiO_2 and B_2O_3 and the phenomena known as the "boron anomaly", where the coordination of boron atoms transitions between trigonal (BO_3) and tetrahedral (BO_4) units. This transition is critically sensitive to the glass composition and affects its macroscopic properties.

CTE is often reduced, while the T_g is increased [66, 70]. These changes can be attributed to modifications in the silicate (Q^n) and borate structural units (BO_4, BO_3) within the glass network as shown in **Figure 2.3**. The addition of alkali oxide promotes the conversion of trigonal BO_3 units to tetrahedral BO_4 units without the formation of NBOs [48]. This change increases the connectivity of the glass network and is typically accompanied by an

increase in T_g. In contrast, in borate glasses, T_g decreases with increasing alkali content, a phenomenon closely associated with the boron anomaly [71]. This contrasting behaviour emphasize the significant differences in structural behaviour between borate and borosilicate glasses and highlights the complex structural interactions when both SiO_2 and B_2O_3 are present in the glass composition. Specifically, alkali oxide-containing borosilicate glasses exhibit a complex network structure because does not experience a similar transition and remains generally free of NBOs. However, with a higher concentration of alkali oxide, the introduction of NBOs into the borosilicate glass structure is unavoidable, leading to further changes in the properties of materials [72]. Alkali and alkaline earth metal oxides generally function as glass modifiers in silicate glasses. However, they can also act as network formers depending on their concentration and the specific glass composition [73]. This dual nature makes understanding the structure-property correlations in glasses containing both SiO_2 and B_2O_3, and multiple modifiers, critical from an application standpoint. Such structure-property correlations are driven by the interplay of factors like which all contribute to the overall material

strength.

Borate glasses are considered for their high transparency, a wide range of glass formation, low melting temperatures, and robust thermal stability [74]. However, borate glasses are known for their low chemical stability, partly due to moisture absorption by boron, and their range of FTIR spectra [75]. These drawbacks can be mitigated through the strategic selection of appropriate modifiers. For example, the chemical durability of borate glasses notably improves with the addition of MgO [76]. Na_20 is also commonly used as a modifier Trivalent oxides, such as Al_2O_3 and Y_2O_3, play a crucial dual role in borate glasses, behaving either as glass formers or intermediates within the matrix [77]. Al_2O_3, in particular, tends to convert BO_3 units into BO_4 units, which leads to an increase in the four-coordinated boron fraction [78]. Consequently, the addition of trivalent oxides to borate glasses has been shown to improve the overall durability, chemical stability, and optical transmission, as well as enhancing water resistance [79]. These additives also strengthen Likewise, the addition of various alkali modifiers to borate glasses causes significant changes in their structural units. When the modifier content is below 30%, four-coordinated boron typically dominates the network. However, with more than 30% modifier content, three-coordinated boron becomes more prevalent, leading to increased NBO formation within the glass network [80]. These changes directly relate to observed changes in the macroscopic properties of glasses.

Therefore, laminated glass has become very common in various structural applications, particularly in the automotive industry due to its enhanced safety features, Understanding its behaviour under impact and crash conditions is crucial for ensuring occupant safety and structural integrity. Consequently, a significant body of research has focused on characterizing, employing both analytical and experimental methodologies.

Several researchers have adopted analytical approaches impact behaviour of [81, 82]. Xu and Li [83] empirically investigated to crash loading. Their findings revealed a direct correlation between impact velocity and crack propagation rates, with both radial and circular crack- ing exhibiting increased rates at higher velocities. These empirical observations provide

under dynamic conditions. Complementing analytical studies, a substantial number of experimental investigations have been undertaken loading scenarios. Such empirical data is essential for validating analytical models and informing design improvements. Furthermore, numerical modelling has emerged as a powerful tool for simulating impact events involving laminated glass. Wang [86] proposed a numerical method to model pedestrian head impact against an automobile windshield, demonstrating reasonable agreement with experimental results. This highlights the potential of numerical simulations to predict impact outcomes and aid in the design of safer vehicle structures. and windshield cracking during impact. This finding offers a valuable parameter for calibrating numerical models and improving the accuracy of impact simulations. Yang et al. [89] utilized Finite Element Method (FEM) through LS-DYNA software to analyze head-windscreen laminated glass collisions, exploring the influence of various factors on impact injury. Jiang [90] focused on reinforcing vehicle safety through purely mechanical structural design. Prasongngen et al. [91] investigated crack behaviour using the element deletion method, concluding that a triangular mesh shape with a size of 1 mm offers a good compromise between accuracy and computational cost in simulating laminated glass behaviour.

Some of the situated findings summarized in **Table 2.2** reveal a strong interdependence between the composition of glasses and their resulting structural, optical, thermal and mechanical properties.

2.5 Motivation of the present study

The optical, thermal, and mechanical properties of glasses play a very important role in the performance of an automotive windshield during its lifecycle. Good mechanical strength, superior abrasion resistance, and excellent optical transmission are key desirable requirements under the performance behaviour of windshield glasses. Commercially available glasses have been tested under defined standard test parameters for their usable life. Geological factors and infrastructure limitations in India are very much responsible for producing abundant dust in the environment around the year. Suspended dust particles not only consist of silicon dioxide and conventional pollutants but also it consists of industrial dust produced by manufacturing units in urban areas, variable carbon content, and dust particles. These particles are responsible for the wear and tear of high-quality braking systems. Improvements in braking materials, a large variety of manufacturing materials used in industries, and increased air and land pollution levels in urban areas have changed over the years, but our testing standards have not been updated accordingly. As a result, actual abrasive materials faced by the vehicles in India are degrading the vehicle's windshield glass to a larger extent as compared to that certified by traditional standard test methods. There is very little evidence available in the literature that has accommodated the changing environmental conditions into the test parameters. There is a huge scope for finding the actual wear behaviour of windshield glasses on Indian vehicles as per the near-actual composition of dust particles faced by the vehicles over the years. Studies of optical, thermal, and mechanical properties tested with near-actual dust loads will provide vital information about the scope of material improvement for improved performance of automotive windshields using conventional mineral oxides.

In addition to this windshield glass, a composite material containing layers of glass and polymer, presents unique challenges and opportunities for recycling. While the glass component itself is readily recyclable, the lamination process and the presence of the interlayer complicate the separation and reuse of materials. Existing recycling methods often result in downcycling or disposal of the entire windshield. This thesis is motivated by the need to develop more effective and sustainable methods for recycling windshield glass and reclaiming valuable materials. Specifically, this research focuses on investigating the properties of recycled glass from windshields. By improving the quality of recycled glass from wind-

shields, this work aims to minimize waste, reduce reliance on virgin materials, and promote a closed-loop system for windshield production and disposal.

2.6 Objectives

- To synthesise silicate-based glasses containing alkali and alkaline earth metal oxides by melt quench technique.
- To investigate the structural, optical, thermal, and mechanical properties of prepared glasses.
- Compare the properties of obtained glasses with commercially available glasses for automotive applications.

Chapter 3

Experimental methods

Overview

This chapter focuses on the details of the glass synthesis and their characterisation using various experimental techniques. the samples using conventional chemicals in powder form. X-ray diffraction (XRD) is used to identify the nature of the synthesised samples, while are used to study the local structural units and change them with respect to wave numbers and composition. The softening and characteristic temperatures are analysed using a dilatometer and respectively to confirm the thermal expansion and glassy nature of the synthesised samples. The elements present in commercially available windshield glasses are analysed a micro Vickers hardness tester, respectively.

3.1 Raw materials

The aim of the present work is to study the structural, optical, and mechanical properties of commercially available windshield glasses and correlate them with their chemical constituents. For that purpose, used and broken windshield panels have been taken from various cars such as Audi A6 Sedan (A6), BMW 7 Sedan (B7), Tata Sumo (TS), Honda Civic (HC), and Maruti Suzuki Swift (MS). The composition of commercially available windshield glasses was investigated using The detailed description of the EDS technique is discussed in **subsection 3.4.3**. EDS analysis of the powder sample was conducted three times across the entire region to ensure uniformity and reproducibility. The obtained data were averaged to enhance accuracy and reliability. amounts in commercially available windshield glasses are given in **Table 3.1** and it is concluded that the windshield glasses are composed of $Si0_2$, Al_20_3, MgO, CaO, Na_20 and K_20. Silica is the main component in most of the windshield glasses.

Based on the EDS findings, the newly optimised glass composition was synthesised using conventional chemicals with the help of the melt-quench technique. Additionally, the above windshield glasses are also recycled and compare their results with the original windshield glass as well as the newly synthesised glasses to check their suitability as windshield glasses.

3.2 Recycling of windshield glass

The windshield of the BMW 7 Sedan (B7) was found to have good transparency, hardness, and fracture toughness [2]. Therefore, the B7 glasses were selected for recycling. The waste glass was ground in an agate mortar pestle with the addition of 1 mol% of B_2O_3, NaCl, KCl, and P_2O_5 in four different batches using acetone as a medium. The samples were mixed thoroughly for 2 hours (h) and subsequently melted at 1550°C in a recrystallised alumina crucible. The glass melting process involved maintaining the furnace at various intermediate temperatures, ranging from 600 to 1200°C for one hour to allow homogenisation and prevent the vaporisation of volatile constituents. The melt was quenched between thick copper plates. This obtained recycled glass is labelled as RB7, RB7B, RB7N, RB7K, and RB7P, containing 1 mol% of B_2O_3, NaCl, KCl, and P_2O_5, respectively. The melting process is given in the flow chart in **Figure 3.3**. However, the presence of elements and their amounts in recycled windshield glasses are given in **Table 3.3**. The obtained glass frits of all the

samples were polished using emery papers of different grades, such as 400, 600, 1000, and 2000, respectively, followed by polishing on a silk velvet with the diamond paste of 6 and 1 µm for 20 minutes each to study their transparency and hardness. For the structural study, the glass frits were ground in an agate mortar pestle to obtain a powder.

3.3 Glass characterisation

The structural, optical, thermal, and mechanical properties of the prepared samples were analysed using various characterisation and measurement techniques. The technical details and adopted parameters during glass characterisation are given in the following sections:

3.3.1 Physical parameters

$$\rho_s = \frac{W_a}{W_a - W_x} \times \rho_{xylene} \tag{3.1}$$

and is a good substance that enters the pores of the glass, which gives proper and precise measurement of density. Moreover, glasses are not soluble in the xylene. The following equation is used to compute the molar volume (V_m):

$$V_m = \frac{M}{\rho_s} \tag{3.2}$$

with a 10 mg minimum count. Some crucial structural characteristics include the oxygen volume (V_e), and (OPD). The following formula was used to determine these parameters after deriving them from molar volume values [3–5]:

$$V_o = \sum_i \frac{V_m}{x_i n_i} \tag{3.3}$$

$$V_e = V_m - \sum_i x_i V_m(i) \tag{3.4}$$

$$OPD = n \times \left(\frac{\rho_{sample}}{M}\right) \tag{3.5}$$

3.3.2 Differential scanning calorimetry (DSC)

The result of a DSC measurement, known as a ther- mogram, is a plot showing the heat flow difference between the sample and reference as a function of the sample temperature, as depicted in **Figure 3.5**.

The thermal stability of windshield glass is a critical property that shows its tendency to

either maintain its amorphous state or undergo crystallisation upon heating. A high degree of thermal stability ensures the retention of optical transparency and structural integrity, rendering it a crucial consideration for applications in optical and high-temperature environments. Specifically, glasses with higher thermal stability are better suited for applications where high temperature is required which prevents the formation of crystalline phases that can degrade performance.

In this study, DSC scans were conducted using a Linseis DSC PT 1600 thermal analyser. The experiments were performed on as-prepared samples under commercial air conditions. During the analysis, a heating rate of 10°C per minute was applied, with Al_2O_3 serving as the reference material in a platinum crucible.

3.3.3 X-ray diffraction (XRD)

X-rays are electromagnetic waves with high energies and wavelengths comparable to the interatomic and interplanar distances (d) in crystals. When an X-ray beam interacts with a solid substance, the electrons associated with each atom in the beam's path scatter portions of the radiation in all directions. Strong scattering occurs only in specific directions that satisfy Bragg's diffraction law for atoms arranged periodically in a lattice. In these directions, the rays undergo constructive interference, resulting in the addition of their amplitudes. This phenomenon is referred to as diffraction when X-rays interact with a crystal. In directions where Bragg's condition is not satisfied, the scattered rays interfere destructively, and reflected or diffracted waves are cancel out each other. For a parallel, monochromatic, and coherent on a set of parallel planes separated by an interplanar spacing d_{hkl}, Bragg's condition for diffraction is expressed by **equation 3.10**:

$$2d_{hkl}\sin\theta = n\lambda \tag{3.6}$$

Here, n represents the order of scattering [6]. converting them into counts per second. The processed data is subsequently displayed on a device, such as a computer monitor, as depicted in **Figure 3.6**. The XRD technique is employed to determine the crystal structure. The angular positions of the diffraction lines provide information about the shape and size of the unit cell. Additionally,

using the unit cell's size, geometry, calculated density, and the sample's chemical composition. X-ray diffraction (XRD) provides both qualitative and quantitative insights into the crystalline phases present in a sample. The diffraction pattern of a phase acts as its fingerprint (FP). Qualitative analysis involves identifying the diffraction pattern associated with a specific crystalline phase. Quantitative analysis in a mixed-phase system relies on the principle that the intensity of a phase's diffraction lines is proportional to its concentration within the mixture [6].

In this study, XRD analysis of finely powdered glass samples was performed using the Rigaku-SmartLab SE ($\lambda = 1.5406$Å), and the software used for XRD measurement is Smart-Lab Studio II. The step size during the experiment was 0.01° and the angular range was between 10° to 80° with a scan rate of 5° min^{-1}. The X-ray source was operated by a 30 mA current and 40 kV accelerating voltage.

Amorphous materials exhibit a broad hump in their XRD patterns, whereas crystalline materials show sharp peaks at Bragg angles corresponding to the diffraction planes characteristic of their crystal structure. Crystallinity is related to hardness and wear resistance, though this often decreases fracture toughness. The changes observed in the amorphous halo, particularly in its position and width, offer insights into modifications in bonding and atomic packing arrangements, as supported by FTIR or Raman spectroscopic analysis.

3.3.4 Field emission scanning electron microscopy (FESEM) and energy dispersive X-ray spectroscopy (EDS)

A field emission scanning electron microscope (FESEM) produces images that provide microscopic-scale information about a sample's morphology, shape, and size etc. This technique relies on the interaction between a highly focused, energetic beam of electrons on the sample which is being analysed, as shown in **Figure 3.7**. During this interaction, energy transfer occurs through either elastic or inelastic scattering. In inelastic scattering, the electron beam transfers part of its energy to the sample, leading to various outcomes: the ejection of weakly bound outer-shell electrons, known as secondary electrons (SE); the removal of inner-shell electrons, resulting in the emission of characteristic X-rays; or the deceleration of the incident beam, producing Bremsstrahlung radiation. In contrast, elastic scattering involves the deflection of the incident electron beam by the atom's electric field without any significant energy loss of the incident electrons. The interactions between the beam and the sample generate backscattered electrons (BSE). BSEs are electrons that undergo elastic interactions with the sample and reverse their direction of travel. The BSE coefficient increases monotonically with the atomic number, allowing local variations in the sample composition to be detected in FESEM-BSE images, a phenomenon known as atomic number contrast. As previously mentioned, SE is produced during the inelastic interaction between the incident beam and the sample. These electrons are emitted from the sample with low kinetic energy (K.E.). Although SE are generated throughout the sample, they lose energy as they propagate, with only a small fraction reaching at the surface. Both SE and BSE provide valuable information about the specimen's topography. These emitted electrons are collected by detectors, typically an Everhart–Thornley detector (sensitive to

both SE and BSE) and a dedicated BSE detector.

are used to determine elemental composition. Since the energies of characteristic X-rays are unique to each element, they serve typically using a semiconductor-based energy-dispersive X-ray spectrometer (EDS) [7]. FESEM provides higher-resolution images of a sample's morphology. The primary distinction between scanning electron microscope (SEM) and FESEM lies in their electron generation systems. While SEM uses a thermionic tungsten electron source, FESEM utilises a field emission gun, which offers significantly greater electron-optical brightness.

Prior to analysis, the samples were prepared in powder form. **Table 3.1** presents the elemental compositions determined through EDS. The EDS analysis allows for the quantification of constituent elements, including SiO_2 and B_2O_3. Higher concentrations of either SiO_2 or B_2O_3 are expected to induce a shift in the Si-O or B-O vibrational modes, respectively, towards higher wavenumbers. This shift indicates an increase in the degree of polymerisation within the glass network. These changes in vibrational modes will be further investigated and confirmed using FTIR or Raman spectroscopy.

3.3.5 Fourier transform infrared (FTIR) spectroscopy

Infrared spectroscopy is an essential analytical technique in materials science, relying on atomic vibrations. When infrared radiation interacts with a sample, certain wavelengths are absorbed while the remaining radiation is structural unit in the materials. For infrared ab- sorption to occur, a change in the electric dipole moment during vibration is required. FTIR spectroscopy is the most widely used technique for infrared analysis. It operates on the principle of inter- ference between two beams to generate an interferogram, a signal that varies with the path length difference between the beams. Fourier transformations are applied to convert the sig- nal between the distance and frequency domains. The incident radiation passes through an interferometer, then through the sample, and finally reaches to the detector. The amplified signal is digitised and processed by a computer to perform the Fourier transformation. The instrument records transmittance as a function of wavenumber. The resulting spectrum can be analysed by assigning specific bands to the vibrations of distinct structural units. FTIR serves as an FP of the sample, which enables the identification of its structural components. Since the absorption wavelength is unique to a particular chemical bond, FTIR can also be used to evaluate the bond's strength. In cases where two or more closely spaced bands

overlap, making it challenging to distinguish spectral features, a signal processing technique called deconvolution is employed. Deconvolution enhances the resolution of the spectrum, allowing for the separation of overlapping peaks and providing a clearer representation of the spectral details [9].

Figure 3.9 demonstrates the sample analysis process using IR spectroscopy, which helps determine and verify the vibrational modes of molecules. Vibrations can occur as bending or stretching within bonds, but not all possible vibrations produce absorption bands in the infrared region. To resolve overlapping spectra that cannot be separated at higher resolution settings, the deconvolution method is applied. By understanding fundamental vibrational modes and deformation types, the more complex vibrations of polymer chains can be analysed. **Figure 3.10** and **Figure 3.11** show the possible vibrational motions of a simple molecule.

To verify the structural modifications and the existence of functional groups, a Shimadzu IRTracer-100 (Shimadzu Corporation, Japan) The FTIR spectrum was recorded using a mixture of sample powder and KBr in a 1:4 ratio. The deconvolution of the FTIR spectra was carried out with Origin 2018

software. are two factors that determine the accuracy of Gaussian fitting, and the values obtained from the fitted data were used to assess the number of bands [4]. The fewest number of bands that results in the maximum value of R^2 (>0.999 in the current study) and the minimum value of χ^2 ($\sim 10^{-7}$ in the current study) were considered to be the necessary number of bands.

FTIR spectroscopy provides a strong response to the characteristic vibrational modes associated with Si-O stretching, BOs, and NBOs within the glass network. Network modifiers, such as Na_20 and CaO, disrupt the glass This depolymerisation effect typically results in a decrease in the vibra- tional frequency observed in both FTIR and Raman spectra. Specifically, (typically observed around 1100 cm^{-1}) shifts towards lower wavenumbers with increasing concentrations of Na_20 and CaO. Complementary Ra- man spectroscopy analysis can further explain the depolymerisation process through changes in the relative intensities of symmetric and asymmetric Si-O-Si vibrational modes.

3.3.6 Raman spectroscopy

Raman spectroscopy operates on the principle of light scattering when it interacts with a molecule and is used to detect molecular vibrations. A laser beam with a single frequency is directed at the sample, and the scattered radiation from the molecule is then measured. The interaction of light with the molecule polarises its electron cloud, causing small frequency shifts. This type of scattering, where no energy is transferred, is called Rayleigh scattering. However, if the scattering results in a transfer of energy between the molecule and the photon, the process is called Raman scattering. Raman scattering is observed as an energy shift from the incident radiation, known as the Raman shift [10]. Raman spectroscopy of the present samples provided additional information on the local structural units in the glasses. The schematic diagram of the Raman spectroscopy principle is shown in **Figure 3.12**.

3.3.7 X-ray photoelectron spectroscopy (XPS)

oxidation states of various ions within a sample. It provides elemental information up to a depth of approximately 10 nm. This method can detect elements ranging from lithium (Li) to uranium (U), provided their concentration exceeds 0.05 atomic% [11].

as shown in **Figure 3.13**. The XPS instrument measures the K.E. of these emitted electrons, as it is directly related to their binding energy (B.E.), which is unique to each element. The B.E. values are then used to generate the XPS energy spectrum as shown in **Figure 3.14**.

$$\text{K.E.} = h\nu - \text{B.E.} \tag{3.7}$$

here, hν represents the energy of the incoming X-ray photon. The XPS instrument consists of three primary components: a source, an energy analyser, and a detector. To ensure accurate measurements, the system operates under ultra-high vacuum conditions [11]. XPS measurements typically employ radiation. Quanti- tative information is derived specific spectral

features.

In the present case, an ultra-high vacuum Thermo Scientific NEXSA surface analysis XPS spectrometer was used, approximately 1.0 eV was used for wide scans, while high-resolution narrow spectra were measured with a step size of 0.1 eV. The wide scans, conducted with a pass energy of 160 eV, helped in identifying peaks and their positions. The peak at 285 eV was used as a reference The analysed powder sample was approximately 10 mg.

XPS analysis of the O 1s core-level spectra enables the differentiation and quantification of BOs and NBOs species within the glass network. An increased NBOs content is indicative of a lower degree of polymerisation, which typically chemical durability of the glass. Therefore, precise control over the BOs/NBOs ratio, as determined through XPS, provides a means to optimise both the mechanical and optical properties of the glass.

3.3.8 Diffused reflectance spectroscopy (DRS)

Diffuse reflectance is a phenomenon utilised in the UV-Vis region to study the optical properties of sample. By analysing the electromagnetic radiation reflected from the surface as a function of frequency, a reflectance spectrum can be obtained the samples. Specular reflection occurs when the angle of incidence equals the angle of re- flection. In contrast, diffuse reflection is characterised by an angle of reflection independent of the angle of incidence. Specular reflection typically occurs on smooth surfaces, whereas diffuse reflection is associated with rough or matte surfaces, such as powders. For powdered samples, the reflected radiation is analysed using a technique known as diffuse reflectance spectroscopy (DRS) [12].

When electromagnetic radiation strikes a surface, it can be reflected (specular), diffracted, refracted, or absorbed. In specular reflection, the radiation interacts solely with the surface. However, the incident beam penetrates the sample in refraction, undergoing multiple reflections and diffractions. If the radiation is not entirely absorbed, it emerges from the sample

and is referred to as Kubelka-Munk reflectance. In principle, both Kubelka-Munk reflectance and specular reflectance occur simultaneously, but only non-absorbing materials can act as ideal Kubelka-Munk reflectors. The Kubelka-Munk theory is based on certain assumptions for deriving its equations. It assumes the absence of a specular reflectance component and that the sample particles are smaller than the overall thickness of the sample. Additionally, the sample must be infinitely thick, meaning the penetration depth of the incident beam should be less than the sample's thickness. It is also crucial to avoid optical effects caused by the sample diameter being smaller than the incident beam. The Kubelka-Munk theory is particularly useful for determining the optical band gap energy (E_g) and it is defined as follows [13]:

$$F(R) = \frac{(1-R)^2}{2R} = \frac{K}{S} \tag{3.8}$$

the value of E_g is determined:

$$F(R)h\nu = A(h\nu - E_g)^n, \tag{3.9}$$

, while n is related to the electronic transitions [15]. When a transition is direct and allowed, n is comparable to 1/2, whereas, for an indirect and allowed transition, it is equal to 2, but when a transition is direct and forbidden, n is comparable to 3/2, while for an indirect and forbidden transition, it equals 3 [16, 17]. The Urbach relation is used to calculate the band tailing's length in localised states [18]. It is expressed as $\alpha(h\nu)=\beta\exp(h\nu/E_u)$, where β is a constant, $\alpha(h\nu)$ is the absorption coefficient as a function of frequency (ν), and E_u is the Urbach energy [19, 20]. From a plot of $h\nu$ (photon energy) on the x-axis and $\ln F(R)$ on the y-axis, a straight line is fitted to the curve and the slope is given as $1/E_u$. The Urbach energy, which reflects the degree of disorder in amorphous materials, is given by the slope's inverse [21]. the relationship between n and E_g are correlated by Dimitrov and Sakka as follows [22]:

$$\frac{n^2 - 1}{n^2 + 2} = 1 - \sqrt{\frac{E_g}{20}}. \tag{3.10}$$

The structural features exert a direct influence on the optical properties of the material. XRD analysis provides insight into the relationship between crystallinity and optical transparency; an increase in the crystalline phase generally reduces transparency due to enhanced light scattering at grain boundaries. Conversely, a more highly polymerised and amorphous structure tends to exhibit greater optical transparency and a larger optical band gap.

3.3.9 Micro Vickers hardness tester

Micro Vickers hardness tester (Mitutoyo, Japan) was used to test the glass samples for hardness with a 2.94 Newton (N) load for a 15-second indentation span. A Vickers hardness tester for a 2.94 N load as shown in **Figure 3.16**. The indentations were made on materials that had not been polished previously.. A light microscope (Eclipse-MA100, Nikon equipment, Tokyo, Japan) was used to measure the indentation dimension for each sample at a magnification of 100. Each load

was subjected to three indentations to avoid error, with the average value recorded. The hardness of samples was calculated using the following equation [23]:

$$H_d = 1.854 \times \frac{L}{D^2} \tag{3.11}$$

where H_d is the hardness of the sample and expressed in GPa, L (N) is The samples were measured by measuring the lengths of cracks that developed as a result of the hardness tests at the indention edges. To confirm that environmental factors did not damage cracks, cracks were measured immediately after applying the load to the specimen. Fracture toughness was calculated using the "halfpenny-crack" formula [24]:

$$F_t = \alpha \times \frac{\sqrt{Y_m}}{H_d} \times \frac{L}{c^{3/2}} \tag{3.12}$$

here c (μm) refers to the half length of the resulting cracks from the centre of the indent while. The modified form of **equation 3.21** is given by Evans and Charles as follows [25]:

$$F_t = \frac{0.0824 \times L}{c^{3/2}} \tag{3.13}$$

A model that takes into account the ionic radii of elements and the bond dissociation energy can be used to calculate the elastic moduli of glasses. Makishima-Mackenzie has presented this concept and developed a useful semi-empirical method for computing Poisson's ratio and Young's modulus based on the glass's chemical composition, the atoms' packing density (V_t), and the bond energy per unit volume (G_t), also known as the dissociation energy.

$$V_t = \frac{\rho}{M} \times \sum_i x_i V_i \tag{3.14}$$

$$G_t = \sum_i x_i G_i \tag{3.15}$$

here, x_i denotes the mole fraction of ith oxide, G_i is defined as the dissociation energy of constituent oxides per unit volume and V_i is the packing factor obtained for respective oxide

constituent A_xO_y as [26]:

$$V_i = N_A \times \frac{4}{3}\pi \times (xR_a^3 + yR_o^3) \tag{3.16}$$

here, N_A is Avogadro's constant while [27, 28]:

$$Y_m = 83.6 \times V_t \times G_t \tag{3.17}$$

$$\sigma = 0.5 - \frac{1}{7.2 \times V_t} \tag{3.18}$$

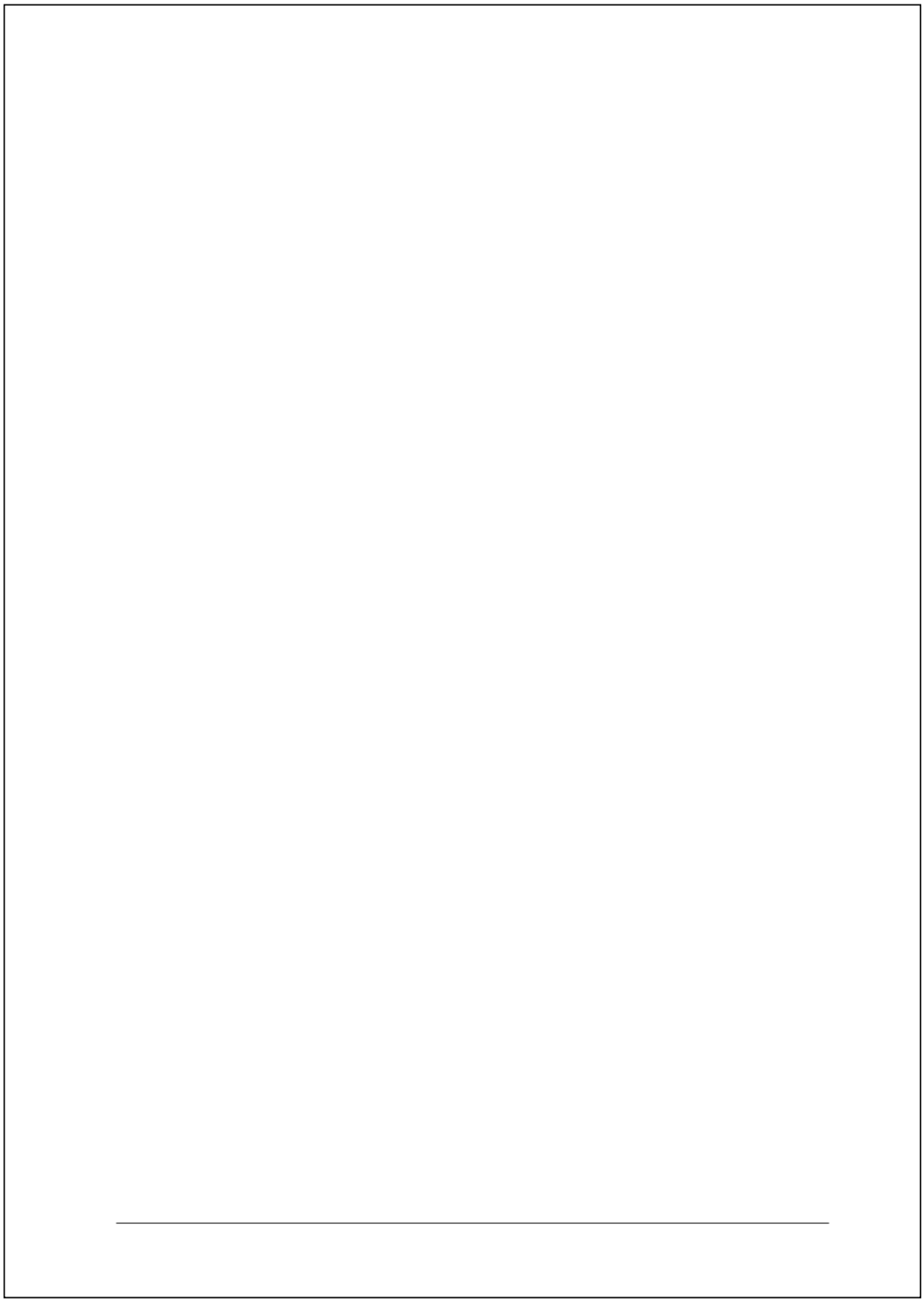

Chapter 4

Results and discussion

Overview

This chapter comprehensively investigates the structural, optical, On the basis of above proeprties three new glass series i.e. $64SiO_2$-$16Na_2O$-$12CaO$-$2Al_2O_3$-$(6-x)MgO$-$(x)A_2O$; (A = Li and K; x = 0, 2, 4 and 6 mol%) and $(64-x)SiO_2$-$(x)B_2O_3$-$16Na_2O$-$12CaO$-$2Al_2O_3$-$6MgO$; (x= 2, 4 and 6 mol%) and testing using various experimental and testing techniques. The obtained results are discussed in light of the chemical nature of constituents, their concentration, process parameters and changes in the glass network and local structural units. Lastly, based on transparency, stability and mechanical properties, four batches of BMW 7 Sedan windshield glass were recycled by adding only one additive in each batch, i.e., 1 mol% of B_2O_3, P_2O_5, KCl and NaCl, respectively, to check their usability and suitability as the windshield glasses in automobiles.

4.1 Chemical and structural analysis of windshield glasses of different cars

4.1.1 FESEM-EDS analysis

The sharp and irregularly shaped particles are observed in FESEM images which are taken on the powder of windshield glass. The powder appeared to have a uniform contrast and brightness with the adjacent particles when the backscattered emission (BSE) images are taken. It confirms the uniform distribution of particles [1] as shown in **Figure 4.1(a)**. The SE image of similar glass samples is also shown in **Figure 4.1(b)**. However, **Figure 4.1(a)** showed some charging effect during the experiment. All the windshield glasses give the same information, whether they were taken in BSE or SE mode of FESEM. Thus, the representative FESEM image of A6 (Audi A6 Sedan) is given in **Figure 4.1**. To know the chemical composition of each windshield glass, the EDS were performed. The chemical composition are given in **Table 3.1** in chapter 3. Ca, Na, Si, Al, Mg, O and K were the major elements present in all the glasses as shown in **Figure 4.2**. All windshield glasses contain SiO_2, Na_2O, K_2O, CaO, MgO, and Al_2O_3.

4.1.2 Physical property

It is noticed that the HC glass has more molecular weight due to the largest concentration of K_20 and Al_2O_3 while the MS glass shows the least molecular weight due to the absence of K_20 and the minimum con- centration of Al_2O_3. HC glass has the highest molecular weight compared to other glasses. The density of glass is strongly affected by changes in glass composition [2]. B7 shows the highest density due to the higher concentration of Na_20 (61.97 g mol^{-1}) while MS shows the least density, which may be due to the absence of K_20 (94.2 g mol^{-1}). It can be linked with various structural unit forms and their interconnection with each other. The variation in molar volume may be due to the creation of NBOs and their connectivity (polymerization) due to the higher concentration of Na_20 in the glass network,

which leads to shrinkage and hence reduces the molar volume. While the higher concentration of K_20 in the HC glass tends to increase the molar volume, which implies an increase in the volume of the glass structure.

4.1.3 X-ray diffraction (XRD) analysis

The XRD patterns of A6, B7, TS, HC and MS are shown in **Figure 4.3**. A lower diffraction

angle between 20°- 30° shows a broad hump in all the XRD patterns. All the glasses exhibit the hump around the same diffraction angle position and are more or less similar in the nature. These XRD patterns confirm the amorphous nature of all the selected glasses.

4.1.4 Thermal analysis

The data obtained from DSC measurements include the glass transition temperature (T_g), crystallisation temperature (T_c), peak crystallisation temperature (T_p), and melting temperature (T_m). The DSC curves for present windshield glasses are shown in **Figure 4.4(a)**. The three distinguishing characteristics of DSC curves are as follows: (a) The values of T_g are indicated by the endothermic peak between 480 and 510°C; (b) the value of T_c is indicated by an exothermic peak between 700 and 750°C; (c) the exothermic peak represents the value of T_p between 750 and 850°C. However, the endothermic peak at a higher temperature range between 1000 and 1200°C designates the T_m. The derivative peak of the TS sample, as depicted in **Figure 4.4(b)**, is utilised to compute the characteristic temperature, and their values are shown in **Table 4.2**.

The structural properties concluded that Al_2O_3 and K_2O play a very important role in polymerisation. It is seen from **Figure 4.4(a)** that these windshield glasses are homogenous in nature. Among all windshield glasses, A6 windshield exhibits the highest (502°C), and MS has the lowest (488°C) value of T_g. A decrease in T_g denotes the formation of NBOs, which

means that the glass structure is less rigid, and the glass network becomes less compact [3]. It may be caused by the prominence of Q^2 structural units in place of Q^3, which generate more NBOs.

$\Delta T = T_c - T_g$ is used to compute the thermal stability factor. An important characteristic of automobile windshield glasses is thermal stability, and the capacity of silicate glasses to withstand heat is essential. The ΔT values for each sample are provided in **Table 4.2**. As per many researchers, glass is said to be thermally stable if its ΔT value is greater than 100°C [4, 5]. Every glass has a ΔT value greater than 100°C. Compared to other glasses, the MS windshield has the highest thermal stability. Therefore, these windshield glasses are thermally stable, and they can bear high-temperature variation as well. Based on the above findings, the three different glass series are proposed to further enhance the required properties of windshield glasses.

4.1.5 FTIR analysis

The weak kink at 2979 cm^{-1} may be due to the O-H stretching vibrations in the hydrogen-bonded dimer [6]. The little kinks observed at 1354, 1711, 2011, and 2176 cm^{-1} which may be due to the multiphonon modes of water free SiO_2 matrix [7]. The windshield of HC is having a little bit higher tendency to contain the hydrogen-bonded dimer in comparison to other windshield glasses. However, it is very low on the windshield of MS. range and the broad

centred around 961 cm^{-1} [9–11]. The availability of more polymerized units like Q^3 is indicated by the broadening and shifting of this transmittance band toward higher wavenumbers. A band at 756 cm^{-1} is due to the Si- O-Si tetrahedral mode of vibration [12]. Because of the broad and asymmetry band between 800-1200 cm^{-1}, deconvolution of the IR spectra is done to know The reduction in deconvoluted band intensity most likely leads to a decrease in network dimensionality [13]. The observations are made that in all the windshield glasses except B7, the Q^3 unit is dominating in comparison to Q^2 and Q^1 silicate units. In B7, the Q^2 unit is dominating in comparison to Q^3 and Q^1 units. In the case of HC, the Q^2 is also a prominent structural unit along with the Q^3 structural units. Whereas Q^2 becomes prominent, the H_20 absorbing tendency is more such as HC and B7 windshield glasses. The K_20 and Na_20 content higher in these windshield glasses may be responsible to convert the Q^3 unit into a Q^2 unit since both are good modifiers. The broadening of the band in the 850-1250 cm^{-1} range

for FTIR transmittance spectra, resulting in the deformation of a Si-O bond length and a reduction in Si-O bond strength, as well as the contrary between Q^n species, an increase in the tiny percentage of NBOs and a reduction in structural connectivity, implying more depolymerized and disordered network structure [14].

4.1.6 Raman spectra analysis

The intensity of all the Raman bands is changed with increasing CaO on the cost of SiO_2 as observed in EDS analysis. The intensity and strength of this

band are enhanced due to the presence of CaO and Na_20 [15]. The broad band in the high-frequency region (900-1250 cm^{-1}) is associated with the Si-O-Si asymmetric stretching vibrations [16]. The peak position at 1092 cm^{-1} does not show any shift by changing CaO with MgO in glass composition [17, 18]. The presence of alkali and alkaline earth oxides in glass broadens the silicate bands, depending on their field strength (F.S.). Higher the F.S. leads to the increase in the broadness of this band (1092 cm^{-1}). The shoulder band is 986 cm^{-1} due to the non-bridging $Si\text{-}O^-$ symmetric vibrations [15]. There is a wide band at 570 cm^{-1} and a less intense band around 793 cm^{-1} in the low-frequency region.

seen near 1100 cm^{-1} is caused by Si-O^- stretching of Q^3 species. Several investigators have found that distinct peaks in this band are deconvoluted to get more detailed information about the structural units. The bands are arranged in such a way that with increasing wavenumber, the degree of polymerization is enhanced. Q^{mn} represents a Q^m unit coupled with a Q^n unit, where m and n represent the number of bridging oxygen in the overlapping region. The vibrations of Q^{33} and Q^{22} tetrahedrons create peaks near 1090-1100 cm^{-1} and 925–950 cm^{-1}, respectively, as well as a line with a maximum at 1010-1040 cm^{-1} due to the vibrations of NBOs atoms in the Q^{32} species. The areas of Q^3 units (Q^{33} + Q^{32}) and Q^2 units (Q^{22}) were measured about the 800-1250 cm^{-1} envelope for quantification of the Q species. It is observed that the Q^3 units increase while Q^2 units decrease with a reduced field strength of modifier cations [20, 21]. The peak deconvolutions have been carried out

for all the windshield glasses. Representative deconvoluted spectra of TS and HC are given in **Figure 4.8(a) and (b)**, respectively.

Based on the deconvoluted results the ratio of Q^3/Q^2 is given in **Figure 4.9**. As obtained from the figure, the highest ratio is observed for TS and the lowest is observed for HC. On the other hand, this ratio is around 5 for the B7 glass. This ratio is low for HC and could be related to intermediate oxides Al_2O_3, about 3 mol% in the composition. It seems that the K_2O played a more important role in increasing the polymerization. As seen in **Figure 4.9**, the ratio of Q^3/Q^2 does not show any regular trend, but it shows variation in TS and HC. The relative area of Q^3/Q^2 is highest in TS, while in HC it shows the lowest value. From this ratio, it suggests that in TS glass, Q^3 is most prominent, while in HC glass, Q^2 is more

prominent. The possible reason behind this variation may be due to 85437. This illustrates the relationship between changes in glass structure and its composi- tion. The highest ratio of Q^3/Q^2 in TS glass as compared to HC glass may be due to the higher concentration of Na_20 in TS. The Na^+ has the highest cationic field strength (CFS) and smallest cationic radius (CR), which results in more attraction towards the NBOs, and leads to the structure becoming more polymerized. While the higher concentration of K_20 in HC glass experiences less attraction towards NBOs due to the lower F.S. and largest CR of K^+. This result is confirmed by FTIR and the optical band gap, which also suggests that more NBOs formed

4.1.7 Diffuse reflectance spectra

The optical band gap due to composition and con- stituents [22]. The presence of K_20, MgO, Al_2O_3, etc. acts as modifiers as well as increasing

the NBOs in the glass network. Due to higher NBOs, B7, HC, and MS show a decrease in their optical bandgap. Interestingly, the B7 and HC glasses have a different trend in comparison to the other glasses, having a lower optical bandgap. This could be attributed to greater disordering caused by higher NBOs produced by modifiers such as Na_2O, K_2O, MgO, and CaO, among others, as already discussed in the FTIR section. Any types of inhomogeneity and NBOs that occur between the conductor and the valence band, might diminish the optical bandgap. The optical band gap of various windshield glasses are given in **Table 4.3**. The samples B7, HC, and MS show a lower bandgap as compared to A6 and TS. -

line earth elements, which caused less charge on NBOs and also increased the ionic nature of the oxygen ions, leading to an increase in the top of the valance bands and a drop in the bandgap [23]. The ionicity of oxygen atoms is increased when BOs are transformed into NBOs. As a result, the top of the valence band shifts up, causing the bandgap to narrow due to increased NBOs [24]. Furthermore, higher atomic number contained modifiers in glass also reduce the optical bandgap [25]. A sample's Urbach energy (E_u) is always smaller than its optical band gap energy (E_g), and an increase in the E_u of the samples indicates that the order of disordering in the samples are also increasing [26–28]. Many factors, including thermal vibrations, NBOs, etc., can influence Urbach tails. In the present glasses, A6 and TS contain the higher Urbach energy, as shown in **Table 4.3**. In the present glasses, more polymerized glass structures are present in B7 and HC as compared to A6, TS, and MS which contain only Q^2 structural units, as also supported by FTIR results of these glasses. The surface shape is the most critical factor in determining the transmittance of any material. B7 and TS had a visible light transmittance of roughly 90% at 400 nm and 86% at 800 nm as shown in **Figure 4.11**. While the standard glass had a transmittance of nearly 90% in the wavelength range of 400-800 nm [29]. Thus, B7 and TS had nearly the same transmittance as standard glass at a particular wavelength, i.e., 400–620 nm. HC and

MS had light transmittances of around 80% at a light wavelength of 400 nm and nearly 60% at 800 nm. While A6 had about 75% at a light wavelength of 400 nm and it gets reduced with time and has a transmittance of about 50% at 800 nm. The correlation between light transmittance and It has the highest Q^2 content, followed by Q^3 and Q^1 structural units, as shown in **Figure 4.6**. The most important result is that the transparency of B7 and TS windshield glasses does not deteriorate as much and is more-or-less constant throughout the variable light spectra range. On the other hand, HC, MS, and A6 show similar behaviour and deteriorate on the higher wavelength side.

4.1.8 Mechanical property

Hardness is complicated and influenced by a variety of parameters, [33]. The com- pactness of the materials is also determined by hardness. The value of hardness for the present windshield glasses lies in the range of 3-5 GPa as shown in **Table 4.4**. The oxide glasses have a Vicker hardness of 2-8 GPa [34]. B7 glass has the maximum hardness i.e. 5.6 GPa. The higher content of SiO_2 usually increases the hardness of the glasses. It is also influenced by the phase separation and process parameters [35, 36]. The hardness measurement of windshield glasses shows that NBO/T is an order that provides value for predicting the hardness of silicate glasses qualitatively.

According to the study, hardness is enhanced with the addition of MgO, while Na_20 exhibits the opposite effect, and the glass network is not as strongly connected with alkali ions, instead with alkaline earth ions [33]. **Table 4.4** shows that the B7 glass has the highest packing density as well as hardness, which may be due to the higher field strength of Na^+ as compared to K^+. A6 has a lower hardness than MS but a higher elastic modulus, which suggests that it has a higher packing density. TS has less hardness than MS but a higher elastic modulus. The fracture toughness is measured by using the crack length that developed along the indentation diagonal as shown in **Figure 4.12**. B7 glass has a higher fracture toughness (1.35 MPa $m^{1/2}$) than other glasses, indicating that the glass used in B7 is more scratch-resistant [37,38].

4.2 $64SiO_2$-$16Na_2O$-$12CaO$-$2Al_2O_3$-$(6-x)MgO$-$(x)Li_2O$; (x = 0, 2, 4 and 6)

4.2.1 Physical property

The additive rule of the mixture is generally followed in density, thus, the replacement of high-density oxide MgO (3.58 g cm^{-3}) in place of the low-density oxide Li_2O (2.01 g cm^{-3}) leads to decrease in the density of the present glasses. The enhancement in the molar volume

(V_m) of the glass can be attributed to the variations in the ionic radii and F.S. of Li^+ and Mg^{2+} ions. The substitution of a Li^+ ion (90pm), which has a larger ionic radius than a Mg^{2+} ion (86pm), leads to an expansion in the glass structure and increases the disordering in the glass network. This conclusion is supported by the Urbach energy as discussed in **subsection 4.2.6**. The excess volume (V_e) and oxygen packing density (OPD) provide a good estimation of the packing density and connectivity of various structural units in the glass. The excess volume shows a variation from the desired mixing volume. It is connected to the compactness as well as the porosity of the glasses [36]. It is observed that the OPD for

as-quenched glasses exhibits an opposite (decreasing) trend than the V_m as shown in **Figure 4.13**. Li^+ reduces the glass network interconnectivity by weakly attracting anions due to its lower field strength, which causes the silicate glass network to become less compact in comparison to glasses containing MgO, resulting in reduced molar volume [39].

4.2.2 X-ray diffraction (XRD) pattern

The XRD patterns for all the Li_20 containing silicate-based glasses are shown in **Figure 4.14(a)**., which suggests that there are no crystalline phases present in these samples. The broad hump between 20°- 30° arises due to the short-range order in the glass [40].

4.2.3 Thermal analysis

The DSC curves for the Li_20 based glasses are shown in **Figure 4.15(a)**. The derivative peak of the SML-4 glass, illustrated in **Figure 4.15(b)**, is used to determine the characteristic temperatures, and their values are listed in **Table 4.6**. T_g rises from SML-0 to SML-2, or with the increase in Li_20 from 0 to 2 mol% as shown in **Table 4.6**. T_g rises as a result of the melt's viscosity becoming more viscous due to an increase in Li_20 content in the

glass melt [41]. The decrease in NBOs in the structure of the glass samples is shown by an increase in T_g [42]. On the other hand, the T_g decreases when the Li_20 content goes from 2

mol% to 6 mol%, or from SML-2 to SML-6. When T_g falls, NBOs are created, which means that modifiers disrupt the glass network and weaken the glass structure [42]. Crystallization combines crystal growth with nucleation. In synthesized glasses, T_p exhibits no clear trend while T_g and T_c follow a decreasing trend, except for SML-2, and this can be due to the mixed modifier effect.

Table 4.6 lists the values of ΔT for each glass. The SML-4 glass exhibits the maximum thermal stability as compared to other glasses. However, the SML-2 and SML-6 samples have marginally the same ΔT, which suggest that with the addition of Li_20 thermal stability shows a slight variation. Moreover, further addition of Li_20 leads to a decrease in the thermal stability. Thus, it can be concluded that the SML-4 glass has high resistance to thermal shock and it prevents from degradation at high temperatures.

4.2.4 FTIR analysis

The entire spectra can be separated into three parts: the high energy part above the wavenumber of 1600 cm^{-1}, the medium energy region 800-1200 cm^{-1}, and the low energy region i.e, 550-750 cm^{-1}. However, at the higher wavenumber side, similar bands are observed as discussed in **subsection 4.1.5**. The change in the band position could be explained by the following equation:

$$\nu = \frac{1}{2\pi}\sqrt{\frac{}{m}} \tag{4.1}$$

where k, m and v are the force constant, mass of the molecule, and lattice vibration frequency, respectively. From the above equation, it is clear that the wavenumber is proportional to $k^{1/2}$. A marginal shift to a lower wavenumber side could mean that the bonds between the different components are becoming weaker with Li_20.

The full width at half maximum (FWHM) of present glasses is increased in the 800-1200 cm^{-1} range when Li_20 is added to it which results in increases in the NBOs in network structure as well as broadens the distribution of Q^n structural units. Therefore, to get a better insight, the FTIR spectra were deconvoluted in **Figure 4.16**. The bands at 896-907 cm^{-1} and 954-973 cm^{-1} belongs to the Q^1 and Q^2 silicate structural units, respectively [43–45]. Moreover, the bands at 1031-1060 cm^{-1} and 1106-1145 cm^{-1} belongs to the Q^3 and Q^4 silicate structural units, respectively [43,46]. When calculating the relative areas of silicate Q^1,

Q^2, Q^3 and Q^4 structural units, the relative areas corresponding to the Si-O-Si asymmetric band are taken into account in order to compute the fraction of silicate Q^1, Q^2, Q^3, and Q^4 structural units. The ratio of (Q^3+Q^1) to Q^2 reveals that when Li_20 concentration rises, the Q^3+Q^1 unit increases instead of the Q^2 structural unit. From this ratio, it can be concluded that the addition of the single valence modifier (Li^+) instead of the double valence modifier (Mg^{2+}) creates asymmetric (odd) structural units, i.e., (Q^3 and Q^1) instead of even ones (Q^2). In order to calculate the fraction (f_1, f_2, f_3 and f_4) of various silicate structural units, the following equations are used [2]:

$$f_1 = \frac{A(Q^1)}{A(Q^1) + A(Q^2) + A(Q^3) + A(Q^4)} \tag{4.2}$$

$$f_2 = \frac{A(Q^2)}{A(Q^1) + A(Q^2) + A(Q^3) + A(Q^4)} \tag{4.3}$$

$$f_3 = \frac{A(Q^3)}{A(Q^1) + A(Q^2) + A(Q^3) + A(Q^4)} \tag{4.4}$$

$$f_4 = \frac{A(Q^4)}{A(Q^1) + A(Q^2) + A(Q^3) + A(Q^4)} \tag{4.5}$$

Based on the values of f_1, f_2, f_3 and f_4, it could be concluded that f_4 decreases with increasing Li_20 concentration and diminishes with the highest content of Li_20, having maximum NBOs as compared to other glasses. Whereas, f_3 and f_2 follow the opposite trend and f_3 and f_1 increase as compared to SML-0. Overall, the f_2 decreases and f_3 and f_1 increaes with Li_20 concentration.

4.2.5 Raman spectra analysis

Two prominent bands are seen in the Raman spectra of glasses in the range of 500-700 cm^{-1} corresponding to O-Si-O bending, and another at about 850-1250 cm^{-1} corresponding to symmetric stretching modes of Si-O bond [47]. On contrary, a weak band is also observed between 700-850 cm^{-1} whose centered at nearly 781 cm^{-1}, corresponding to the Si-O-Si symmetric stretching vibrations of isolated SiO_4 tetrahedral with four NBOs i.e, Q^0 [43]. As compared to SML-0, with an increase in the Li_20 concentration, the FWHM also increased from 102 to 107 cm^{-1}, the band becomes broadened with Li_20 and shifts towards higher wavenumber side in the range of 500-700 cm^{-1}, which indicates that the Li_20 contained

glasses exhibit higher disordering than SML-0 glass [48] as shown in **Figure 4.14(c)**.

At the higher band 1250-1000 cm^{-1}, SML-2 shows a marginal shift towards the lower wavenumber. It means the bond length increases by increasing the Li_2O in glasses. While, at the lower side 500-700 cm^{-1}, the band intensity, as well as the area of SML-2, are very low this anomalous behavior could be related to the mixed modifier effect [22, 35, 49]. Similarly to FTIR, the Raman spectra of each glass are also deconvoluted into individual bands as given in **Figure 4.17**. The multiple bands obtained after deconvolution correspond to the symmetric stretching of the Si-O bonds with different NBOs [50–52]. Q^1 and Q^2 structural units related to 948-956 cm^{-1} and 1006-1039 cm^{-1}, respecteively. However, Q^3 and Q^4 structural units related to 1075-1089 cm^{-1} and 1153-1163 cm^{-1}, respectively. The $(Q^3 + Q^1)/Q^2$ ratio varies from 1.14 to 27.80, and this ratio is highest for glass SML-6 and lowest for SML-2. With respect to the undoped glass (SML-0), it is observed that with an increase in the concentration of Li_2O, the odd units $(Q^3 + Q^1)$ increase instead of the even ones (Q^2),

which is also supported by FTIR results as discussed in the previous section. Whereas, glass SML-2 shows unusual behaviour, which may be due to the mixed modifier effect. Bands present between 500-700 cm^{-1} after deconvolution in the as-quenched glasses are caused by the bending vibrations of SiO_4 tetrahedral with three bridging oxygen molecules (Q^3) [53].

4.2.6 Diffuse reflectance spectra

Diffused reflectance spectra are performed to analyze the optical characteristics of the Li_20 based glasses (powder form). As shown in **Figure 4.18(a)**, $(F(R)h\nu)^2$ vs hν graphs were extrapolated to reach the x-axis equivalent to $(F(R)h\nu)^2 = 0$. The calculated band gap energy values lie in the region and vary from 3.88 to 4.03 eV, as shown in **Table 4.7**.

modifications caused by lithium over the magnesium control the variation in the optical band gap [54, 55]. The SML-6 glass has the smallest band gap (3.88 eV), and the SML-0 glass has the largest band gap (4.03 eV). The band gap decreases with an increase in the F.S. of Li^+ in the composition (shown in **Table 4.7**) resulting in an increase in the NBOs. It is well-reported that NBOs decrease the optical band gap in the glasses. The composition of the glass samples also affects the refractive index (n). The quantity of NBOs has a significant impact on the refractive index since donating an electron is also necessary for NBOs formation. As the amount of Li_20 rises, the refractive index increases to its maximum for SML-6. It can be observed that n and E_g are inversely proportional to each

other. The glass's refractive index is influenced by its density, coordination number, and NBO content. More ionic bonds are created during the formation of NBOs, which increases polarizability and raises the band gap of the material [56]. Thus, the possible reason for this trend to more NBOs being produced when Li_20 is added. **Table 4.7** lists the values for the optical band gap along with Urbach energy. A glass's band gap energy is always greater than its Urbach energy [23]. With an increase in Li_20 concentration, the Urbach energy also increased. Higher Urbach energy means higher disordering in the glasses [26]. It was observed that the SML-6 glass had the highest Urbach energy value

As-quenched glass samples were measured for light transmittance in the visible range 400-700 nm as shown in **Figure 4.18(b)**, and it was found that the undoped glass SML-0 had transparency, around 84% at 400 nm and 88% at 800 nm. Whereas Li_20 content increased the transparency, it only reached 86% at 400 nm and 88% around 800 nm in glass SML-4. It was observed that the highest Li_20 contained glass, i.e., SML-6, had the highest transparency, around 87% at 400 nm and 90% at 800 nm, compared to other glasses. Moreover, transparency increases continuously between 400 and 700 nm. From this result, we conclude that with an increase in the concentration of Li_20, the glass structure becomes more open, due to which the most amount of light gets passed through the glass. The light transmittance for commercially available soda-lime-silicate glass (SLG) is also about 90% [90]. Raman spectra and the physical characteristics of the current glasses also support this conclusion. On the other hand, glass SML-2 shows an unusual trend as compared to other lithium-doped samples. It had a transparency of around 81% at 400 nm and 86% at 800 nm, which is also less than the even SML-0 (x=0 mol%). The possible reason behind

this unusual behaviour is the polymerisation of the network structure in glass SML-2, as per the conclusions drawn from the Raman spectra of these glasses. In other lithium-doped samples, the Q^3 and Q^1 structural units are most prominent, while in glass SML-2, the Q^2 unit is more prominent than the Q^3 and Q^1 units. It could be associated to the mixed modifier effect. Since it is more pronounced where both the modifiers' ratios tend to become ~ one [22, 56]. It seems that the asymmetric creation of SiO_2 unit i.e, Q^3 and Q^1 increases the transmittance in the visible region of the present synthesized glasses.

4.2.7 Mechanical property

Vicker's indentation testing can be used to determine the hardness (H_d) and fracture toughness (F_t) of the glasses. **Table 4.8** provides the measured H_d value that correlate to the diagonally indentation lengths. It was observed that a sample SML-0 has a hardness of nearly 6.70 GPa, but with an increase in the concentration of Li_20, hardness decreases. Probable of this fall in hardness is associated with NBOs, which is clearly evident from the. In the glass network, there is an inverse relationship between microhardness and NBOs. NBOs decrease the interconnectivity of the glass network, thus lowering the microhardness of the glasses [58]. Since hardness represents and it is frequently correlated with cation [59].

As the F.S. of the Li^+ (1.73/Å^2) is lower than Mg^{2+} (3.85/Å^2), thus, it has a low polarizing power and less attractive force toward the NBOs. By determining the length of the crack

(c) that develops at the indenter's corner, the fracture toughness of the material can be observed. It has been noted that the glass SML-0 has a higher F_t due to the higher CFS of Mg^{2+}. In the glass SML-0, the glass Mg-O bond [60]. As the concentration of Li_20 increases, the glass network becomes weak and more NBOs will be formed. It is clear from **Table 4.7** that SML-6 has lower F_t due to the lower F.S. of Li^+, which forms a higher number of NBOs and leads to less attraction between cations and NBOs. The equation given below was used to determine the brittleness index (B_i) for each glass [61–63]:

$$B_i = \frac{H_d}{F_t} = \frac{22.505 \times c^{3/2}}{L^2} \tag{4.6}$$

Densification and plastic deformation flow patterns that take place prior to the fracture initiation stage determine the brittleness of the glasses [63, 64]. However, it is considered that the brittleness index of silicate glass is about 9 $\mu m^{-1/2}$ [65]. the brittleness of the as-quenched glass samples increases, and this may be due to the lower amount of densification in the glasses (mentioned in **subsection 4.2.1**). While glass SML-2 shows an unusual trend, it may be due to the mixed modifier effect that was observed in the Raman spectroscopy, as well as the transmittance of this particular glass. In the present glasses, the observed values also fall within the range of reported values. This shows that when the amount of Li_20 increases, the glass network's strength decreases. This variation is attributed to the fact that the Li_20 may be weaker in the glass network because MgO has a higher field strength than Li_20, its higher contribution in glass SML-0 increases its binding capacity, leading to an increase in the elastic modulus.

4.2.8 XPS analysis

XPS has been performed on selected glasses (SML-0 and SML-6) to analyze the details of the oxygen (O) situation. **Figure 4.19** shows the XPS spectra of SML-0 and SML-6 glasses. In the Si 2p high-resolution XPS spectrum (**Figure 4.19(c)**), the peak shifts to the lower binding energy for the SML-6 glass containing the higher concentration of Li_20

(x=6 mol%), suggesting weaker interactions between Si- [66, 67]. Alkali ions (R^+) change molecules ($Q^4 \rightarrow Q^3$), where Q^n and n corresponds to the the number of BOs, respectively.

$$-Si-O-Si-+Li_2O \rightarrow -Si-O-Li^+ + -Si-O-Li^- \quad (4.7)$$

Lithium oxide in this reaction splits the bound Q^4 units into two Q^3 units. The Q^4 units are covalently bound together, whereas the Q^3 units are The Si-O bonds tend to weaken due to the low F.S. ($1.73/Å^2$) of Li, which alters The shift of the Si 2p peaks indicates that the corresponding Si-O bond weakens with increasing R-NBO bond strength [67]. The SML-0 and SML-6 glasses show two peaks of O 1s lines as shown in **Figure 4.19(a) and (b)**. The 0_{NBR} (non-bridging oxygen) atoms are responsible for the O 1s line's intensities, which are growing with increased Li_20 concentration. contained in the Si-O-Si bonds correspond to the high-energy O 1s-line. It is

observed that of NBO increases, which leads to the formation of Li-NBO bonds and weakens the glass network.

4.3 $64SiO_2$-$16Na_2O$-12CaO-$2Al_2O_3$-$(6-x)$MgO-$(x)K_2O$; (x = 2, 4 and 6)

4.3.1 Physical property

The density of all the glasses decreases from 2.52 to 2.49 g cm^{-3} with an increase in the concentration of K_2O in place of MgO. It could be due to the lower density of K_2O (2.35 g cm^{-3}) as compared to MgO. In addition to this, the substitution of K^+ (1.38 Å), with a larger ionic radius, for Mg^{2+} (0.72 Å), with a smaller ionic radius, causes the expansion of the glass network structure has higher effect than mass change which increases the volume of the glass. The lower density decreases the scattering of light, hence increasing the transparency of glasses. In principle, there is an inverse correlation between molar volume and density; with a decrease in molar volume, density always increases [68, 69]. As a result, SK-6 had

---

the lowest density among all the glasses and had the greatest molar volume. In this series, V_m of the as-prepared glass samples increased with K_2O content. This is mainly due to the large size and smaller cation field strength of K^+ (0.52 $Å^{-2}$), which makes the network

less compact than a glass network containing Mg^{2+} (3.85 $Å^{-2}$) [56]. Because of this, more space is available in the glass matrix. The molecular mass is directly proportional to V_m, as shown in **equation 3.2**. A possible reason for the increase in molecular mass in the present composition is the replacement of the lower molecular mass MgO (40.3 g mol^{-1}) by the higher molecular mass K_2O (94.2 g mol^{-1}). An increase of the K_2O content raised the V_m values and production of excess free volume. The open structure may increase the transparency of the glass as discussed in **subsection 4.3.6**. The observed variation in V_e might have been caused by modifier ions that were present in the glass network's interstices.

As shown in **Table 4.9**, an inverse trend is observed between OPD and V_m, and a possible reason for the drop in OPD with an increase in the concentration of K_2O is the reduction in oxygen atom/constituent in a proportion of 1:2, which causes fewer connections in the glass network [70]. Because of this, the structure of the glass becomes even more extended and loosely packed, which results in a reduction in stiffness with lower cross-linked networks, which leads to an. The inverse link between the two factors supports K_2O acting as a more pronounced network modifier than MgO in the present glass network.

4.3.2 X-ray diffraction (XRD) analysis

Figure 4.20(a) displays the XRD patterns of all the K_2O based glasses. A broad halo between 20° and 30° is observed in all the glasses, which confirms with the addition of K_2O in place of MgO, which could be related to the local glass structural units [71]. It could be correlated to the addition of K_2O, which may increase the degree of ionic bonding as compared with the degree of covalent bonding and it may be due to the larger cationic radius of K^+ (1.38 Å) in comparison with Mg^{2+} (0.72 Å). As a result, by substitution of K^+, with a larger cationic radius, for Mg^{2+}, with a smaller cationic radius, local structural units develop in the SMK-2 diffraction pattern [71].

4.3.3 Thermal analysis

The DSC curves for the synthesized glasses are shown in **Figure 4.21(a)**. The derivative peak of the SK-6 glass, illustrated in **Figure 4.21(b)**, is used to determine the characteristic temperatures, and their values are listed in **Table 4.10**. The physical and structural properties concluded that the addition of K_20 in place of MgO weakens the glass network and decreases its compactness. It is seen from **Figure 4.21** that K_20 significantly affects the characteristic temperatures of the glasses. Out of all the glasses, SMK-2 has the highest T_g value (591°C), whereas SK-6 has the lowest (560°C). When K_20 concentration increases from 2 mol% to 6 mol%, is observed. is degrading and the glass network is breaking, as indicated by the drop in T_g, which also indicates the creation of NBOs. It may be caused by the transformation of Q^2 structural units into $Q^3 + Q^4$ silicate structural units in the SK-6 glass which generates more NBOs. This alteration weakens network connectivity

thermal stability. Raman spectroscopy analysis indicates that the polymerization index decreases with increasing K_20 content. This reduction in polymerization suggests a shift in the struc- tural network, likely due to the increased presence of Q^2 units at the expense of Q^3 and Q^4 units. Higher thermal stability can also be associated with higher crosslinking which can show an adversely affect on transparency by introducing light-scattering domains. However, the SMK-2 glass demonstrates high resistance to thermal shock and effectively prevents degradation at higher temperatures.

4.3.4 FTIR analysis

The FTIR spectra of this series, as shown in **Figure 4.20(b)**, are more or less similar as discussed in **subsection 4.2.4**. The tendency of the K_20 contained glass to absorb water molecules is higher than Li_20 contained glasses. The Si-OH related tiny bands at 2000-2300 cm^{-1} are more strongly evident for the above-mentioned reasons. It is increased with the concentration of K_20. The Si-O-Si link is disrupted, permitting the production of the silanol group at about 2010, 2176, and 2274 cm^{-1} [72].

$$Si{-}O{-}Si + H_2O \rightarrow 2SiOH \tag{4.8}$$

The silanol group formation in the present glasses is also beneficial to improve the adhesion and wetting behavior of the glass since windshield glass has a polymeric layer between

the two layers of glass. So, the present glasses could be a good choice for automobile applications. With an increase in the K_2O concentration, this band shifts to a higher wavenumber and becomes broader. A shift to a higher wavenumber signifies a strengthening of the bonds between the various constituents [73]. In addition to this, the uniformity of the chemical bonding affects the FWHM. The band locations are slightly affected by changes in bond length. On the other hand, because of the variation in the FWHM, the band between 820 and 1200 cm^{-1} becomes broad with K_20, which could be associated to the greater cationic size of K^+ than Mg^{2+} [74, 75]. At around 937 cm^{-1}, the most intense band is seen in spectra. It is related to asymmetric stretching vibrations of Si-O-Si. In this instance, various structural units are also located in this area. Because there are several structural units and linkages present, and because of the crossing of the bands, this band is more intense, and its minimum shifts toward a higher wavenumber with increasing K_20 concentration in the glass. In the as-prepared glasses, the transmittance band at around 756 cm^{-1} is assigned to the Si-O-Si symmetric stretching vibrational mode. The area of the FTIR transmittance spectra in the 820-1200 cm^{-1} region was used to define the distribution of structural units Q^n; thus, the 820-1200 cm^{-1} region, was deconvoluted as shown in **Figure 4.22**. The bands corresponding to 905 cm^{-1}, 915 cm^{-1}, and 926 cm^{-1} belong to the Q^1 silicate structural unit, the bands corresponding to 1002 cm^{-1}, 1019 cm^{-1}, and 1039 cm^{-1} belong to the Q^2 silicate structural unit, and the bands corresponding to 1121 cm^{-1}, 1141 cm^{-1}, and 1133 cm^{-1} belong to the Q^3 silicate structural unit. In this particular band, Q^1, Q^2, and Q^3 are related to the structural units that are present in silicate glass. The variation in Q^2/Q^1 confirms that with an increase in the concentration of K_2O, the content of the Q^1 unit increases relatively to the content of the Q^2 unit, and because of this, NBOs also increase in number in glasses with increasing K_2O concentration, depolymerizing the glass network and weakening the glass structure because of reduced cross-linking and bond breaking by the modifiers.

4.3.5 Raman spectra analysis

Raman spectroscopy was used to further confirm the findings from the FTIR spectra, and **Figure 4.20(c)** shows the Raman spectra of all the as-prepared glasses. The Raman bands are very similar to the Li_2O contained glasses except for some broadness and shift of the peak. To get more information, the deconvolution has been done on the Raman spectra. Band deconvolution of Raman spectra was done to understand more about the Q-unit distribution in the 850-1250 cm^{-1} region, where there is a maximum at approximately 1086 cm^{-1}. In the 850-1250 cm^{-1} region, several other bands are also present, at 940-950 cm^{-1}, 1010-1070 cm^{-1}, 1080-1100 cm^{-1}, and 1130-1170 cm^{-1}, as shown in **Figure 4.23**. These bands correspond to the Si–O symmetric stretching vibrations for the SiO_4 tetrahedral configuration, i.e., the Q^2 structural band for SiO_3^{2-}, the Q^1 structural band for $Si_2O_5^{2-}$, and the Q^0 structural band for SiO_2^0, and these tetrahedral configurations form a 3D network because of the linkages at all corners of the tetrahedral unit [76]. To take the

interconnectivity of the silicate tetrahedra into consideration, various studies were conducted in accordance with the literature [77,78]. With an increase in the degree of depolymerization, the obtained band contains various cross-linkage structural units, which are described as Q^{21} (cross-linking between Q^2 and Q^1 units), which corresponds to 948, 946, and 949 cm^{-1}, Q^{22}, which corresponds to 1009 cm^{-1}, Q^{32}, which corresponds to 1041 and 1065 cm^{-1}, Q^{33}, which corresponds to 1094, 1089, and 1078 cm^{-1}, and Q^{43}, which corresponds to 1152, 1133, and 1169 cm^{-1}. The existence of these bands is due to the NBOs in silicate tetrahedra sharing various coordination spheres with the modified cations [79]. The areas of the Q^2 units (Q^{21} + Q^{22}), Q^3 units (Q^{32} + Q^{33}), and Q^4 units (Q^{43}) were calculated. It is expected that the Raman scattering cross sections between the remaining Q^n species should not differ too much for the modified glasses with relatively comparable glass compositions [80]. However, it was observed that the fully polymerized Q^{43} silicate tetrahedron's Raman scattering cross section, as seen in the as-prepared glasses, is incredibly small in comparison [81].

F.S. cation Mg^{2+} is replaced by the lower F.S. cation K^+, the intensity of the Q^3 unit becomes higher as compared with that of other units, which may cause an increase in the relative population of the Q^3 groups relative to the Q^2 and Q^4 groups in the present glasses. To gain more insight into the Raman spectra, the area as a factor of the level of network disproportion was also calculated. divided into three equal parts, denoted by the formula $A(Q^2)/A(Q^3 + Q^4)$. When the field strength of the modifier cations decreases, the $A(Q^2)/A(Q^3 + Q^4)$ ratio rises. This illustrates the relationship between changes in glass composition and glass structure. The relative number of Q^3 and Q^4 species declines as the fraction of Q^2 species rises with the K_2O concentration. From this ratio, it is concluded that with an increase in the concentration of K_2O in place of MgO in the present glasses, the Q^2 unit becomes more prominent than the Q^3 and Q^4 units. Because of this, these glasses are less polymerized, and hence the FTIR results are also confirmed as discussed in **subsection 4.3.4**. Additionally, Si–O bond lengths for NBO ions are greater than for bridging oxygen ions, and this variation increases as the modifier content rises [83]. According to Brawer and White's analysis of the Raman bandwidths [84],

the disorder in glasses rise as cation size of modifier ion increase i.e., $K^+ > Na^+ > Li^+$. Similar results are observed in the present glasses

The microstructure of such a silicate glass can be learned through the examination of its Raman spectra. The relative strengths of the bending and stretching bands, according to the theory of Labet and Colomban [47], can give an excellent estimate of the degree of polymerization. With use of this concept as a foundation, a polymerization index (I_p) was developed as the ratio of the area of the bending band at nearly 500 cm^{-1} to the area of the stretching band

at nearly 1000 cm^{-1}:

$$I_p = \frac{A_{500}}{A_{1000}} \tag{4.9}$$

It is observed that I_p decreases with an increase in the concentration of K_2O and shows a minimum value for the glass with x = 6 (SK-6). Modest I_p values indicate low levels of polymerization, whereas high I_p values indicate high levels of polymerization. According to the theory of Labet and Colomban [47], a lower I_p corresponds to an increase in the number of NBOs per silicon atom, and this result also supports the results obtained for the present glasses. A similar trend is also observed in Li_20-containing glasses, which suggests that in alkali-based silicate glasses, polymerisation index decreases with an increase in the concentration of alkali oxides.

4.3.6 Difused reflectance spectra

E_g for SMK-2 is 3.97 eV, which decreased to 3.89 eV for SK-6 as shown in **Table 4.11**. However, as mentioned in the previous discussion, the SK-6 glass exhibits more NBOs than the other two glasses. Thus, the addition of K_2O produces more NBOs in the present glasses. the optical band gap to reduce, which raises the top of the valence band and makes oxygen ions more ionic [85]. This type of trend was also observed by Bansal et al. [86]. Moreover, the value of E_g is comparable to the Li_20 containing glasses.

E_u for an SMK-2 glass was measured as about 0.39 eV, while the SMK-4 and SK-6 glasses show an increase in trend in Urbach energy (E_u). For SK-6, the highest value of the Urbach energy was observed. It is evident from this that SK-6 has greater disordering than the other glasses. Actually, E_u is an expression of material imperfections. The FTIR and Raman spectra of SK-6 are more diffuse and broader than those of the other glasses, which further supports the presence of more imperfections.

SMK-2 and SMK-4 have nearly the same value of n, i.e., 2.17, because of only a slight change in the content of K_2O, while SK-6 has the largest refractive index, i.e., 2.19. The production of NBOs increases with the effectiveness of the modifier (lower field strength). The number of ionic bonds increases as the number of NBOs increases in the system, which is also explained by physical parameters. A higher refractive index results from the greater ionicity [87]. The refractive index of windshield glass is in a similar range of approximately 2.24-2.28 [88]. However, the refractive index of Li_20 and K_20 containing glasses are nearly the same.

The most important parameter affecting any material's transmittance is its surface profile [89]. **Figure 4.24(b)** illustrates the light transmittance of the as-prepared solid glass samples. It is seen that SK-6 has the highest transparency, around 83% at 400 nm and 87% at 800 nm. It is very interesting that the transparency increases between 400 to 800 nm. However, it is less than for the windshield glass of BMW 7 series and Honda Civic cars as we reported previously [88]. At 400 nm, the light transmittance of SMK-2 and SMK-4 was almost 80%, while at 800 nm, it was around 83% for SMK-4 and 81% for SMK-2. Compared with the other samples, SK-6 had greater light transmittance, which may have been caused by an open network structure due to which the maximum amount of light passes through the sample, and this conclusion is supported by the Raman spectra as well as the physical parameters of the present glasses. SK-6 has the largest Q^2 content relative to Q^4 and Q^3 content. The transparency of the as-prepared glasses does not degrade and is more or less constant across the visible range, which is the most significant result [89].

4.3.7 Mechanical property

A possible reason for this variation is the smaller F.S. of K^+ (0.52 $Å^{-2}$) as compared with Mg^{2+} (3.85 $Å^{-2}$). The cation F.S. of different constituents in glass plays a crucial role to modify or form the glass network [56]. K^+, having a larger cationic radius than Mg^{2+}, which has a lower attraction, corresponds to the weakest F.S. from the oxygen that is not bridging [90]. While K^+ generates more of its coordinate linkages, however, it does not appropriately strengthen the structure because of its connection with NBOs. Consequently, SMK-2 had the highest hardness, when MgO is present in the maximum amount. Since SMK-2 has a stronger link, there is a greater attraction between the bonds. As a result, SMK-2 glass demonstrates better hardness among all the glass samples. The observations strongly demonstrate that modifiers affect the fundamental quality of glasses. This is because their F.S. varies, which eventually affects the local configurations of ions in a glass matrix. With an increase in the concentration of K_2O in the as-prepared samples, the packing density and the elastic modulus both decrease, which may be due to the larger size of the K^+ ion occupying the volume to a greater extent. The densely packed structure demonstrates the maximum elastic modulus as well as hardness, which is observed from

Table 4.12. This type of variation in Y_m and V_t has also been reported by many researchers [86, 90]. The hardness of the present glasses is comparable to the hardness in our earlier reports, as well as that of commercial windshield glasses [56, 88, 90, 107].

4.4 (64-x)SiO_2-(x)B_2O_3-16Na_2O-12CaO-2Al_2O_3-6MgO; (x= 2, 4 and 6)

4.4.1 Physical property

The addition of B_2O_3 in place of SiO_2 in the above series decreases the density with increasing B_2O_3 content. The molar volume (V_m) values steadily rise as the B_2O_3 content increases in the glass composition.. Furthermore, the rise in oxy- gen atoms in a unit's chemical composition is responsible for the increase in oxygen molar volume (V_o). The increase in OPD suggests that the glass network becomes compact with the addition of B_2O_3. However, the other two glass series show a reverse trend in OPD thus, it can be concluded that OPD is the most suitable parameter to determine the compactness of glass structure.

The compactness and the expansion of the glass network can be explained by the network

volume (NV). The term NV is defined as the volume occupied by 1 mole of network-forming units that are often found in glass. The formula used to compute this quantity is defined as follows:

$$NV = \frac{SiO_2\% \times M_{SiO_2} + B_2O_3\% \times M_{B_2O_3} + Na_2O\% \times M_{Na_2O}}{\rho \times (SiO_2\% + 2 \times B_2O_3\%)} + \frac{CaO\% \times M_{CaO} + Al_2O_3\% \times M_{Al_2O_3} + MgO\% \times M_{MgO}}{\rho \times (SiO_2\% + 2 \times B_2O_3\%)} \quad (4.10)$$

where M is the molar mass of the oxide designated by the subscript in the equation. It is observed that 62S-2B glass has the highest (35.63 cm^3 mol^{-1}) NV, followed with the other two glasses as given in **Table 4.13**. The variation in NV with the addition of B_2O_3 resulted in a contraction of the glass network which leads to the greater contraction effect.

4.4.2 X-ray diffraction (XRD) analysis

It is observed from the XRD patterns that broadly diffused scattering at low angles (between 20° and 40 The broad hump between 20° and 40° due to the short-range structural units [86]. This outcome also shows that these compositions have good glass-forming capabilities.

4.4.3 Thermal analysis

Figure 4.26(a) shows the DSC curves for as-prepared glasses. The peak of the derivative curve, as shown in **Figure 4.26(b)**, is used to calculate the T_g, T_c, and T_p. The values for T_g, T_c, T_p, and T_m for as-prepared glass samples are shown in **Table 4.14**. No trend is observed in the characteristic temperatures of the present glasses. The addition of B_2O_3 in SiO_2 enhances the compactness and makes the glass network strong, which was concluded in the structural as well as mechanical sections. The behaviour of T_g is found to be controlled by other modifiers, despite B_2O_3 having a significant impact on the T_g of these glasses. In the synthesised glasses, 60S-4B has the lowest (534°C) while 58S-6B has the highest (543°C) value of T_g. It might be driven by the development of BO_3 and BO_4 units, which alter the glass structure by introducing NBOs into the network. On the other hand, due to the presence of other modifiers, BO_3 converts into BO_4 without forming NBOs in the 58S-

6B glass, and this change increases the network connectivity, which leads to an increase in T_g [42]. However, in the present samples, characteristic temperatures do not follow any trend, and this can be due to the boron anomaly. In view of this, the borate anomaly produces a nonlinear trend in thermal and optical properties when the glass former's composition is altered while the modifier remains constant in the glass composition. In the manufacturing of these glasses, it is necessary to sandwich a polymer layer so that it can bear maximum load, as well as during accidents glass would not be shattered easily [88]. Thus, the fibre drawing is a reheating process that requires very high temperatures, it is ideal for a glass host to have as much space as possible in order to establish a wide working range of temperatures during the manufacturing of windshield glasses. In **Table 4.14**, the values of ΔT are listed for each glass. All glasses exhibit ΔT value higher than 100° C. 62S-2B glass has the highest thermal stability than other glasses. Thus, these glasses can be suitable candidates for automobile applications.

4.4.4 FTIR analysis

The bands mainly relate to various vibrations of the borate and silicate units. The, 1409 cm^{-1}, 1501 cm^{-1}, 1715 cm^{-1},
1997 cm^{-1}, 2247 cm^{-1}, 2875 cm^{-1}, 2879 cm^{-1}, 3006 cm^{-1}, and 3674 cm^{-1} are visible in are visible in the other two glass series as well. However, borate glasses typically include hydroxyl groups; thus, in this glass series, small bands are present in the higher wavenumber side, which can be due to the OH groups.
According to the literature [91–93 bonding configurations are responsible for the FTIR bands that correspond to the fingerprint region (400-1500 cm^{-1}

(H_2O) group. absorbing moisture from the surrounding environment [94]. The band at 1715 cm^{-1} is due to the stretching

mode of the hydroxyl group. The band at 3006 cm^{-1} is due to hydrogen bonding. With the increase in B_2O_3 content, the tendency to absorb moisture from the surroundings decreases in glass samples. The bands at 2879 cm^{-1} and 2875 cm^{-1} are due to the stretching mode of the hydrogen-bonded O-H group. The band at 2247 cm^{-1} is attributed to the O-H group. Borate glasses typically include hydroxyl groups. The band at 1997 cm^{-1} is due to the stretching mode of the O-H group. The O-H group is associated with weak hydrogen bonds which form NBOs in a glass matrix. While the band at 1501 cm^{-1} is due to the asymmetric stretching modes of the B-O bond and B-O^- in the borate triangle BO_3 unit. More BO_3 is generated with 58S-6B, as seen by the increased intensity of this band for 58S-6B compared to the other two glasses. The band center is at 953 cm^{-1} due to the vibration of the B-O and Si-O units. The B-O and Si-O bands are marginally near each other. Due to varying units, combined bands may occasionally overlap. That's why deconvolution is conducted for the region between 1400- 800 cm^{-1} in order to distinguish between the various structural units.

The band at 771-772 cm^{-1} is due to the bending mode of Si-O-Si. Bands at nearly 901-912 cm^{-1} and 976-1014 cm^{-1} are ascribed to Q^1 and Q^2 structural units, respectively. The band at 1077- 1133 cm^{-1} is associated with the Q^3 silicate structural unit. This indicates that the higher BOs are present in 58S-6B glass and decrease for 60S-4B, followed by 62S-2B glass.

4.4.5 Raman spectra analysis

The Raman spectroscopy results further validate the FTIR spectrum findings, and the spectra of all the glasses are displayed in **Figure 4.25(c)**. Several small bands around 489, 573, 628, and 783 cm^{-1} and broad bands between 830 and 1300 cm^{-1} are characteristic peaks for borosilicate glass. According to the literature [95–99], the band at 489 cm^{-1} is due to the mixed stretching and bending modes of Si-O-Si units. The band at 628 cm^{-1}

corresponds to the 4-fold ring, containing two SiO_4 and two BO_4 tetrahedra. However, this band shows splitting into 573 cm^{-1} due to the Si-O-Si bond's stretching mode. The band at 783 cm^{-1} is due to the four-coordinated boron in diborate and boroxyl rings. In order to get more clarity about the structure of the glass, deconvolution was done in the range of 830-1300 cm^{-1}. The bands are designated based on their positions, specifically Q^1, Q^2,

and Q^3 which are depicted in **Figure 4.28**, are based on silicon structural arrangements with oxygen. Bands at nearly 958 cm^{-1} and 1068 cm^{-1} with 1 and 2 BOs designated by Q^1 and Q^2, respectively. The band between 1080-1110 cm^{-1} with 3 BOs assigned to Q^3. With the addition of B_2O_3, the intensity of band Q^2 decreases, whereas the intensity of band Q^3 increases, which suggests that the glass network becomes more polymerized. However, it is also observed that there is a slight shift in the structural units, and this shift follows the non-linear trend, which is due to the boron anomaly. The boron anomaly is observed in the optical and thermal properties as well.

4.4.6 Diffuse reflectance spectra

The E_g of glasses is found to be in the insulator range (3.95-3.84 eV) as shown in **Figure 4.29(a)**. The optical band gap without B_2O_3 exhibited
4.03 eV as given in **Table 4.7**. It is observed that the E_g initially decreases (upto 4 mol%) and further increases (above 4 mol%). It has been observed that the E_g decreases with an increase in B_2O_3, which leads to a rise in bonding defects and NBOs. The reduction in the E_g with higher B_2O_3 content is attributed to structural changes in the material. This causes increased electron localization, which in turn raises the number of donor centres in the glass matrix. The increase in donor centres results in a further reduction of the optical band gap. It might be because there are more NBOs in the 62S-2B glass,

and this result is also supported by structural properties as discussed in **subsection 4.4.4**. The present samples do not follow any trend with the addition of B_2O_3. This non-linearity in E_g and E_u can be due to the mixed glass former effect due to the presence of both SiO_2 and B_2O_3 as formers in the glass [100].

As-quenched glass samples were measured for light transmittance in the visible range of 400-700 nm as shown in **Figure 4.29(b)**, and it was observed that sample 62S-2B had transparency, ~ 83% at 400 nm, which increases continuously and reaches upto 88% at 800 nm. Whereas with an increase in the concentration of B_2O_3, transparency decreased in the glasses, and it reached a minimum of 82% at 400 nm and 86% at 800 nm for sample 58S-6B. SiO_2 and B_2O_3 both are glass network formers. However, the cationic field strength of B_2O_3 (41$Å^{-2}$) exhibits higher than SiO_2 (25$Å^{-2}$). So, the network becomes more compact after adding B_2O_3 in place of SiO_2 which leads to a decrease in the interaction between light and glass. So, the transparency is going to decrease with B_2O_3 content. From this result, it concludes network becomes more compact, due to which the least amount of light gets passed through the glass. Structural as well as physical properties are in support of this conclusion. Although the prepared glass samples have distinct optical transmittance, however, this has no effect on the glass's visibility.

4.4.7 Mechanical property

Table 4.16 displays the values of Poison ratio (σ) obtained for the present glasses, which vary from 0.247 to 0.244. This suggests that the behaviour of the synthesised glass samples is approaching a The possible factor for increasing the stiffness in glass samples with increasing B_2O_3 is that B-O has a bond strength of 499 kJ/mol, which is higher than that of Si-O (444 kJ/mol).

The 62S-2B glass has the lowest hardness (6.03 GPa) while the 58S-6B glass has the highest hardness (6.94 GPa). The value of hardness and fracture toughness are found to be similar

by other researchers [35, 86]. As compared to commercially available windshield glasses and the other two series, the as-prepared glasses have more hardness [88]. The hardness without B_2O_3 exhibited 6.70 GPa as given in **Table 4.7**. When B_2O_3 is incorporated in place of SiO_2, the hardness get decreases. However, with an increase in the concentration of B_2O_3, the hardness increases. The increase in hardness is due to the decrease in NBOs, which make the glass network more compact, and it is clearly evident from the structural as well as physical properties of the present glasses. NBOs open the glass network and decrease the interconnectivity, which leads to the indenter penetrating deeper inside the sample at a specific load. Thus, the hardness of the glasses decreases with an increase in the penetration depth [58, 86].

The length of the crack (c) that emerges from the indenta- tion's corners can be used to determine the fracture toughness. Silicate glasses usually have a fracture toughness of around 0.7 MPa $m^{1/2}$ and with the presence of different dopants, it could rise to 1 MPa $m^{1/2}$ [103]. The 58S-6B glass has the highest Young's modulus (69.06 GPa), while the 62S-2B glass has the lowest Young's modulus (68.98 GPa). The highly packed structure has the highest Young's modulus as well as the highest hard- ness. The silicate glasses with Young's modulus lie in the range of 50-130 GPa [104].

It is observed that with an increase in the concentration of B_2O_3, fracture toughness increases except for the 62S-2B glass. The unusual behaviour of 62S-2B can be attributed to the open and planar structure of B_2O_3. The addition of the BO_3 planar triangle in the SiO_4 tetrahedral struc-

ture makes the network structure open, and due to this, after the indentation, no radial cracks developed around the corners of the indentation. Further increases in the content of B_2O_3 develop the radial cracks around the indentation, and they can be due to the higher bond strength of B-O (499 kJ/mol) as compared to Si-O (444 kJ/mol) which leads to the network structure become more compact and increase the fracture toughness [105].

brittleness decreases with an increase in the concentration of B_2O_3 except for 62S-2B glass. This is estimated because B_2O_3 acts as a glass former to decrease the discontinuity of the glass network, which leads to stronger bonding and decreases the brittle behaviour of the glasses. The sample 62S-2B shows unusual behaviour because B_i depends on F_t due to this, there is no brittleness index observed for this sample. When describing the fracture resilience of brittle materials, fracture toughness is frequently used. A material's ability to withstand the propagation of cracks is known as fracture toughness. The substance with a higher fracture toughness is less brittle [102].

4.5 Recycling of windshield glass

As discussed in the **section 4.1**, the B7 glass represents the optimised properties which are essentially required to qualify the glass for automotive applications. Based on the obtained results, B7 glass is recycled to check its feasibility for reuse in automobiles. So, for that, 1 mol% of different additives are added in the used windshield glasses. The additives are added to decrease the bubbles and increase their effect on the properties, particularly transparency. Moreover, the obtained results of recycled glasses are compared with the present research work.

4.5.1 Physical property

The RB7P glass has the highest molecular weight due to the molecular weight of P_2O_5 (141.94 g mol^{-1}) is the highest among all other components. However, the density of the RB7P sample is highest in comparison to the other samples, and this could be due to the

higher concentration of Al_2O_3. Since Al_2O_3 density (3.95 g cm^{-3}) is higher than other constituents of glasses., it is obvious that the addition of B_2O_3 results in the least density of the RB7B glass, which could be due to the lower concentration of K_2O. The addition of NaCl and KCl might break in Na^+, K^+, and Cl^-. However, Na^+

and K^+ react with oxygen and form Na_2O and K_2O whereas, Cl^- reacts with Si and forms the $SiCl_4$ as given in **equation 4.12**. This leads to the highest density of RB7P among all other samples. In the RB7B glass, the molar volume is highest, which indicates that with the addition of B_2O_3, the glass, network is extended, which leads to an increase in the and this leads to the least dense glass as compared to other glasses.

4.5.2 X-ray diffraction (XRD) analysis

The XRD pattern of the recycled glasses is depicted in **Figure 4.30(a)**. The absence of any significant peaks, suggests that these glasses do not include any crystalline phases, which confirms that all of the glass samples are amorphous in nature. There is a broad hump

between 15°-40° and it can be due to the presence of short-range order or silicate network in the recycled glass [107]. When NaCl and KCl are added to the recycled glass, the contraction of the nearby glass structural units causes this broad halo to shift marginally towards a higher diffraction angle. All the samples exhibit only one halo, indicating the formation of homogeneous glasses.

4.5.3 FTIR analysis

FTIR transmittance spectra of the recycled glasses with various modifiers (CaO, Na_20, MgO, K_20, and Al_2O_3) are shown in **Figure 4.30(b)**. The bands at the higher wavenumber side, i.e. above 1200 cm^{-1}, give the same information as shown in **Figure 4.25(b)**. The band between 1200-800 cm^{-1} is the fingerprint region and is connected to asymmetric stretching vibrations of the Si-O-Si bond in silicate glasses that are linked to varying quantities of oxygen atoms that bridge. This band shifts to the somewhat higher wavenumber

side when 1 mol% of B_2O_3 and KCl are incorporated in it. The shifting in the RB7K glass is due to the highest concentration of CaO as compared to other recycled samples while the shifting in the RB7B glass is due to the highest concentration of Al_2O_3 as compared to the RB7K glass. However, NaCl brings a slight modification in the fingerprint region, which shifts the band side is due to the lower concentration of SiO_2 as compared to other recycled samples. It is known that in vibrational transitions, the wavenumber varies correspondingly to $\sqrt{k/m}$, and here k and m have their usual meanings [108]. The dominance and strengthening of the relationships between the various components is shown by a shift to the higher wavenumber side [109]. It seems that "k" is more dominant than "m" with the incorporation of different oxides. The effect of NaCl, KCl, B_2O_3, and P_2O_5 in the present composition is seen in the region of 800-500 cm^{-1}. It is observed that the band at 762 cm^{-1} shifts to the lower wavenumber side,

Deconvolution of the spectra, i.e., the 1300-600 cm^{-1} range, was done because of the wide spectra and to confirm the existence of more bands, as seen in **Figure 4.31**. Based on the deconvolution, it is possible to conclude that, f_2 and f_4 show an increasing trend whereas, f_1 and f_3 show the reverse trend. f_2 and f_4 are highest in the RB7P glass, in which P_2O_5 is incorporated by 1 mol%, which leads to the result that with the addition of P_2O_5, the glass network gets closer together, and additionally, the possible reason for an increase in the value of f_2 and f_4 is due to the highest concentration of Al_2O_3 as compared to other recycled samples. This conclusion is also supported by the RB7P glass as discussed in the previous section. To confirm the contribution of silicate units in the recycled glass composition, the ratio was taken between $Q^2 + Q^4$ and $Q^1 + Q^3$. It is observed that alumina (picked from an alumina crucible) plays an important role in this recycled glass composition, which polymerises the glass network and increases the sym- metrical units of the silicate network. As seen in **Table 3.3**, the concentration of Al_2O_3 is highest in the RB7P glass, due to which the $Q^2 + Q^4$ are more prominent units as compared to $Q^1 + Q^3$ units.

4.5.4 Raman spectra analysis

Broad bands between 900-1200 cm^{-1} and several tiny bands around 465, 588, 796, and 1410 cm^{-1} are the distinctive peaks for silicate-based glasses [110, 111]. These tiny bands are similar and give the same information as B_2O_3 containing glasses, as shown in **Figure 4.25(c)**. The deconvoluted Raman spectra in **Figure 4.32** in the range of 400-1300 cm^{-1} also show several additional bands. The existence of various bands is implied by the high-frequency asymmetric band because of the many structural units and cross-links among the units (charge-balanced silicate tetrahedra). The band centre shifts to lower wavenumbers at 1080 cm^{-1} when the concentrations of B_2O_3, NaCl, KCl, and P_2O_5 are incorporated in the present composition. Deconvolution was carried out in the 400-1300 cm^{-1} range to provide

better clarity regarding the glass's structural units. These curves provide the most accurate portrayal of glasses across multiple vibration bands.

Bands with 2 and 3 BOs were identified by Q^2 and Q^3, respectively, at roughly 945-982 cm^{-1} and 1029-1081 cm^{-1}. The band at 1125-1162 cm^{-1} with four BOs designated as Q^4. The deconvoluted band present at the lower wavenumber side, i.e., 460-477 cm^{-1} is because of the Si-O-Si bond's combined stretching and bending [3]. However, in the RB7P glass the band at 454 cm^{-1} is due to the bending of the O-P-O in PO_4^{3-} unit [41]. The band at 500-600 cm^{-1} is due to the mixed stretching and bending vibration of the Q^3 and Q^4 units [107].

The $(Q^2 + Q^4)/Q^3$ ratio varies from 0.27 to 3.25 and it is observed that when 1 mol% of

B_2O_3, KCl, and P_2O_5 are incorporated in RB7, the even units (Q^2 + Q^4) rise rather than odd ones (Q^3) except for RB7N glass and this unusual behaviour of RB7N glass is due to the highest concentration of CaO in this glass. It is already reported that a double valence modifier usually creates symmetrical (even) structural units (Q^2 and Q^4) [108]. These observations are validated by the FTIR data (**subsection 4.5.3**). However, RB7N glass exhibits anomalous behaviour that could be because when NaCl is added, the intensity of the Q^2 and Q^4 units falls while Q^3 rises, which implies a decrease in the polymerisation of the glass network instead of other samples. Upon recycling, Na^+ actively participates to enhance the formation of Q^3 units instead of Q^2 and Q^4, while B^{3+}, K^+, and P^{5+} enhance the formation of Q^2 and Q^4 units, which makes the glass network more rigid, which leads to an increase in density except for the RB7B glass as shown in **Figure 4.33**. The glass network of RB7 and RB7K samples can be visually realised as shown in **Figure 4.34(a) and (b)**. This explains the compactness in the structure, decrease in the molar volume, and increase in the density of recycled glasses.

4.5.5 Diffuse reflectance spectra

It is observed from **Table 4.18** that the band gap lies between 3.35 and 3.50 eV, and it is highest for the RB7 glass (3.50 eV) while lowest for the RB7B glass (3.35 eV). It is reported in the range of 3.20-3.80 eV [112, 113]. This behaviour might be related to the structural alterations brought about by the addition of B_2O_3. Additionally, the concentration of NBO atoms rises upon the addition of B_2O_3 during the recycling of the glass. As a result, the glass structure becomes less ordered, as supported by the E_u values, and the addition of B_2O_3 results in the breakage of the regular structure of silicate (creation of NBOs), which lowers the band gap [114, 115]. Additionally, with the incorporation of B_2O_3, the increment in NBOs, which bind excited electrons less strongly than BOs [116]. However, with the addition of NaCl and KCl, the band gap of RB7N and RB7K glasses is nearly constant, which is due to the marginally similar value of the band gap (~ 8 eV) for NaCl and KCl [117, 118]. It can be concluded that the RB7 glass has the highest band gap, which supports the highest polymerization. On the other hand, the RB7B glass has the lowest band gap, which is associated with its lower polymerization.

The E_u increases with the addition of B_2O_3, which suggests that more defects are introduced in the RB7B glass, and this could be due to the lower contribution of Q^3 and Q^4 structural

units as compared to the RB7 glass. As a result, B_2O_3 strongly tends to convert weak bonds into defects, leading to increased Urbach energy. The incorporation of NaCl and KCl in recycled glasses shows the highest value of Urbach energy in RB7K glass, which concludes that KCl creates more defects instead of NaCl. The possible reasons could be due to the higher contribution of Q^2 units instead of Q^3 and Q^4, which creates more NBOs in the glass network. However, it is observed that P_2O_5 reduces the value of Urbach energy due to a higher contribution of Q^4 units. From the above result, it could be concluded that a decrease in the Urbach energy leads to a decrease in the degree of disorder in the glass structure [119].

RB7B and RB7P glasses have the highest refractive index (n), which re formed in these glasses as compared to other recycled glasses. The RB7 glass has a lower value of "n" due to a lower concentration of Al_2O_3. As the concentrations (1 mol%) of B_2O_3, NaCl, KCl, and P_2O_5 are incorporated in the RB7 glass,

the value of the refractive index increases due to the increase in the concentration of Al_2O_3. The structural properties show that more ionic bonds form in the system with an increase in NBOs. The increased ionicity has the effect of raising the refractive index. It is already reported that soda lime silicate-based glasses in the range between 2.18 and 2.25 [107,115].

The recycled glasses were subjected to visible light measurements in the range of 400-800 nm, as illustrated in **Figure 4.35(b)**. The results showed that the RB7 glass exhibited a transparency of around 90% at 400 nm, which decreased steadily to 85% at 800 nm. It concludes that after recycling, the transparency is more or less similar to the BMW 7 Sedan (B7) glass as reported earlier [115]. In contrast, transparency is decreased as the concentration of B_2O_3, NaCl, KCl, and P_2O_5 are incorporated in recycled glasses. It is observed from **Figure 4.36** that as the fraction of $Q^1 + Q^2$ units increases, the transparency of the RB7B glass decreases, and it can be due to the higher content of f_2 as compared to f_1. Due to this, the network of glass gets increasingly dense, which leads to an increase in the interaction of light with glass, and as a result, a minimum amount of light is allowed through the glass [2, 3, 120]. However, the fraction of Q^1 and Q^2 silicate units further increases instead of Q^3 and Q^4, which makes the glass network more weak and open. Due to this, the interaction between the light and glass decreases, and consequently, the glass allows

the most light to travel through it. Thus the transparency increases up to the RB7K glass. After this again, the fraction of $Q^1 + Q^2$ units decreases which means the structure becomes more compact due to an increase in the fraction of $Q^3 + Q^4$, which makes the network more compact due to this low interaction between electromagnetic waves and glass. This conclusion is also supported by the structural and physical properties of RB7P glass. As a result, the transparency of the RB7P glass decreases. Interestingly, at higher wavelengths, the transparency of RB7B, RB7N, and RB7K deteriorated except for the RB7P glass, in which transparency became more or less constant.

4.5.6 Mechanical property

Optical micrographs of the microcracks and Vickers indentations that developed on the RB7 and RB7K glasses are shown in **Figure 4.37(a) and (b)**. Every glass sample that was subjected to a force of 4.90 N for 15 seconds showed signs of breaking Radial and median cracks were seen on the RB7 and RB7K glasses; however, the Vickers notch has developed circular cracks as shown in **Figure 4.37**.

According to **Table 4.19**, the hardness value for the current glasses is between 4.29 and 5.74 GPa. The observed mechanical properties are directly correlated with the fraction of silicate units as shown in **Figure 4.38**. It is observed that with the addition of B_2O_3, NaCl, KCl,

and P_2O_5, the value of hardness decreases as compared to RB7 glass. This decrease in hardness is due to the increment in fraction of Q^1 and Q^2 silicate units instead of Q^3 and Q^4, which leads to a less densely packed glass network.. NBOs contribute to opening up the glass network and reducing interconnectivity, hence permitting the indenter to delve more into the sample at a specific load. Consequently, the hardness of the glasses diminishes as the penetration depth increases [58]. From the **Figure 4.38**, it can be concluded that with an increase in the fraction of Q^1 and Q^2 silicate units, upto the RB7K glass, the structure becomes less polymerized, due to which the hardness of recycled glass samples decreases. However, after the RB7K glass, the fraction of Q^1 and Q^2 silicate units decreases, which

means the structure gets polymerized which leads to a rigid glass network and increases the hardness of the RB7P glass.

The value of F_t increased when dopants like B_2O_3, NaCl and KCl were incorporated in the pristine glass sample. However, with the addition of P_2O_5 the value of F_t decreased. Among all the glasses, RB7P exhibits the highest Young's modulus at 83.34 GPa, while RB7 has the lowest Young's modulus at 64.18 GPa. Interestingly, the densely packed structure corresponds to the highest Young's modulus and hardness. Silicate glasses typically possess Young's moduli within the range of 50-130 GPa [115, 121]. The brittleness of the glasses is determined by densification and plastic deformation flow patterns that occur before the fracture initiation stage. With the addition of glass formers (B_2O_3 and P_2O_5) and fining agents (KCl and NaCl), the recycled samples become less brittle, which may be because the glass samples have undergone more densification. It is observed that the molar volume decreases (**Table 4.17**), which leads to increases in the atomic packing density.

The Young's modulus of glass is 71.4 GPa, which was reported by Lu et al [124]. However, the silicate glasses with Young's modulus lie in the range of 50-130 GPa [121]. Adding additives like B_2O_3, NaCl, KCl and P_2O_5 increased Young's modulus due to an increase in the coordination in the glass network [123]. Loose or packed atom matrices affect the glasses' elastic modulus. The elastic properties of oxide glasses showed that they were highly dependent on the microstructure and chemical

composition of the glasses [33].

4.5.7 XPS analysis

XPS is a very good tool to estimate NBO and BOs in better ways than the other techniques. All samples underwent XPS survey measurements to determine their elemental compositions. **Figure 4.39(a)** which belongs to the RB7B and RB7P glasses as representative, revealing the presence of Si, Al, B, O, Na, K, Mg, Ca, P and C. The presence of carbon might be attributed to surface contamination. The elemental composition of the selected glasses are shown in **Table 4.20**. In the high-resolution Si 2p

spectrum, a shift to higher binding energy is observed for the RB7P glass as shown in **Figure 4.39(b)**, which is due to the higher concentration of Al_2O_3. This shift suggests stronger Si-O interactions. The shift in the Si 2p peak indicates the strong Si-O bond as the strength

of the R-BO bond increases. However, the presence of alkali (Na^+, K^+) and alkali (Ca^{2+}, Mg^{2+}) ions modify the silicate structure, changing it from Q^4 to Q^3 while Al_2O_3 which is an intermediate oxide and acts as a network former which leads to increases the connectivity in the glass. Thus, it can be concluded that the presence of P_2O_5 and Al_2O_3 influence the polymerization process and alter the optical as well as mechanical properties of the glasses., high-resolution O 1s spectra have been analyzed for the selected samples. **Figure 4.39(c) and (d)** shows the deconvolution of O 1s peak for the RB7B and RB7P glasses, respectively. The non-bridging oxygen (O_{NBR}) atoms contribute to the O 1s line intensities, which decrease with the addition of P_2O_5. In contrast, the bridging oxygen (O_{BR}) atoms within the Si-O-Si bonds are associated with the high-energy O 1s line. As the concentration of P_2O_5 is incorporated, the BO intensity increases, promoting the formation of P-BO bonds and strengthening the glass network.

Summary

Based on the previous findings, the important parameters which are required for the windshield in automobile applications are given below. The **able 4.21** represents the optical band gap (E_g), transparency in the visible range (400-800 nm), microhardness (H_d) and fracture toughness (F_t) of windshield glasses, as-prepared as well as recycled samples.

Chapter 5

Summary of the thesis

This chapter contains the major conclusions of the present research work. The future scope of studies evolved from this work is also given in brief.

Windshield glasses of different cars are taken from an automotive repair shop to investigate their structural, optical, thermal, and mechanical properties correlated with their chemical constituents. It is observed that the highest transparency, hardness, and fracture toughness are observed for BMW7 Sedan as compared to other windshield glasses due to moderate contents of Al_2O_3 in its composition. Composition-tuned glasses with varying amounts of alkali and borate oxides have been synthesised via the melt-quench technique. The above-discussed properties of the synthesised glasses were examined to determine their suitability for applications in automobile windshield glasses. In addition to this, small quantities of glass formers and fining agents such as B_2O_3, P_2O_5, NaCl, and KCl are added to recycle the BMW 7 Sedan windshield glass and study their effect on various properties.

The major conclusions drawn from the study of the structure-property correlation of the synthesised glasses are as follows:

- Lower field strength and lower binding energy of modifier ions with NBOs significantly decrease the packing density of structural units of glasses, which decreases the hardness of the glasses.
- The presence of different silicate structural units in the synthesised glasses exhibited a more disordered glass structure as compared to the commercially available windshield glasses, which consist of silicate structural units only. However, the presence of B_2O_3 enhanced compactness in glass structural units.
- The non-linearity in the properties were influenced by the mixed modifier effect and boron anomaly in glasses.
- The glass transition temperatures of the synthesised glasses are in the desired range, exhibiting suitability as a windshield in automobile applications.

- SML-6 had the highest transparency, ~ 87% at 400 nm and 91% at 800 nm as compared to other glasses. Moreover, transparency continuously increases between 400 and 800 nm as compared to commercially available windshield glasses.

Based on the recycling of the B7 windshield glass, the presence of Al_2O_3 and P_2O_5 was found to significantly influence the polymerisation process and thereby impact the optical as well as mechanical properties of the recycled glasses. This study paves the way for clean and environmental friendly recycling and reusable windshield automobile glasses without compromising their original properties.

Future scope

- Other alkali and alkaline earth oxides, such as PbO, SrO, and BaO, are contained in silicate glasses that can be synthesised and investigated for their optical and mechanical properties with the present research work
- $64SiO_2$ - $16Na_2O$ - 12CaO - $2Al_2O_3$ - $6Li_2O$ (SML-6) is a suitable candidate which can be used in automobile applications.

Santosh_Thesis_KUS2

ORIGINALITY REPORT

7%	3%	5%	1%
SIMILARITY INDEX	INTERNET SOURCES	PUBLICATIONS	STUDENT PAPERS

PRIMARY SOURCES

1	www.mdpi.com Internet Source	<1%
2	Savidh Khan, Santosh Kumar, Shahbaaz Khan, Km Abida, K. Singh. "Influence of ZrO2 on non-isothermal crystallization kinetics, structure and optical properties of calcium borosilicate glasses", Materials Today Communications, 2024 Publication	<1%
3	Submitted to University of Sheffield Student Paper	<1%
4	Musariri, John. "Luke-Acts Mission Paradigm for the Church in the Socio-Economic Context of Southern Zimbabwe", University of Pretoria (South Africa), 2024 Publication	<1%
5	lib.buet.ac.bd:8080 Internet Source	<1%
6	moam.info Internet Source	<1%
7	worldwidescience.org Internet Source	<1%
8	open.metu.edu.tr Internet Source	<1%
9	assets.researchsquare.com Internet Source	<1%

08/07/2024
(Dr. Prabal Pratap Singh Bhadauria)

10	"Atomistic Simulations of Glasses", Wiley, 2022 Publication	<1 %
11	www.researchgate.net Internet Source	<1 %
12	Jagpreet Singh, Vishal Kumar, Yogesh K. Vermani, M.S. Al-Buriahi, Jamila S. Alzahrani, Tejbir Singh. "Fabrication and Characterization of Barium based Bioactive Glasses in terms of Physical, Structural, Mechanical and Radiation Shielding Properties", Ceramics International, 2021 Publication	<1 %
13	Osama Bagi Aljewaw, Zhi Wei Loh, Mohd Hafiz Mohd Zaid, Sharudin Omar Baki et al. "Exploring the Optical, Structural, and Gamma Shielding Performance of Dy_2O_3-Doped Li_2O–B_2O_3–Al_2O_3 Glass Systems", Materials Chemistry and Physics, 2025 Publication	<1 %
14	Submitted to University of Wollongong Student Paper	<1 %
15	Abuzer Acikgoz, Gokhan Demircan, Demet Yılmaz, Bulent Aktas, Serife Yalcin, Nuri Yorulmaz. "Structural, mechanical, radiation shielding properties and albedo parameters of alumina borate glasses: Role of CeO2 and Er2O3", Materials Science and Engineering: B, 2022 Publication	<1 %
16	Ajitanshu Vedrtnam, S.J. Pawar. "Laminated plate theories and fracture of laminated glass plate – A review", Engineering Fracture Mechanics, 2017 Publication	<1 %

17	dokumen.pub Internet Source	<1 %
18	Gao Qu, Zhiwei Luo, Weizhen Liu, Anxian Lu. "The preparation and properties of zirconia-doped Y–Si–Al–O–N oxynitride glasses and glass-ceramics", Ceramics International, 2013 Publication	<1 %
19	Olga N. Koroleva, Vsevolod N. Anfilogov, Anton Shatskiy, Konstantin D. Litasov. "Structure of Na2O–SiO2 melt as a function of composition: In situ Raman spectroscopic study", Journal of Non-Crystalline Solids, 2013 Publication	<1 %
20	Yuhang Zhou, Jiacheng Li, Huidan Zeng, Long Zhang. "Physical and elastic properties of Gd2O3-regulated gallate glasses", Materials Today Communications, 2023 Publication	<1 %
21	"Technological Advances in Tellurite Glasses", Springer Science and Business Media LLC, 2017 Publication	<1 %
22	Millena Lograd, Yara Hellen Firmo Gomes, Tomiki Inoue, Shingo Nakane et al. "Densification of sodium and magnesium aluminosilicate glasses at ambient temperature: structural investigations by solid-state nuclear magnetic resonance and molecular dynamics simulations", Physical Chemistry Chemical Physics, 2024 Publication	<1 %
23	m.moam.info Internet Source	<1 %
24	Abd El-Moneim, A.. "Structural role of RO and Al"2O"3 in borate glasses using an ultrasonic	<1 %

technique", Acta Materialia, 200608
Publication

25	Khagendra Baral, Aize Li, Wai-Yim Ching. "Ab Initio Modeling of Structure and Properties of Single and Mixed Alkali Silicate Glasses", The Journal of Physical Chemistry A, 2017 Publication	<1 %
26	Tou Ying Lim, H. Wagiran, R. Hussin, S. Hashim, M.A. Saeed. "Physical and optical properties of dysprosium ion doped strontium borate glasses", Physica B: Condensed Matter, 2014 Publication	<1 %
27	pubs.rsc.org Internet Source	<1 %
28	"Emerging Photovoltaic Materials", Wiley, 2018 Publication	<1 %
29	Sakthi Prasad, Anustup Chakraborty, Kaushik Biswas. "Chapter 8 Melt-Derived Bioactive Glasses: Approaches to Improve Thermal Stability and Antibacterial Property by Structure–Property Correlation", Springer Science and Business Media LLC, 2022 Publication	<1 %
30	Neetu Bansal, Mukul Gupta, Bhaskar Chandra Mohanty, Kulvir Singh. "Evaluating the role of composition and local structure on alkali out-diffusion in glasses for thin-film solar cells", Journal of the American Ceramic Society, 2020 Publication	<1 %
31	dr.ntu.edu.sg Internet Source	<1 %
32	repository.library.carleton.ca Internet Source	<1 %

33	Submitted to National Institute of Technology Karnataka Surathkal Student Paper	<1 %
34	Submitted to University of Central England in Birmingham Student Paper	<1 %
35	Zhiwei Luo, Gaorong Han, Anxian Lu. "Zn–Sr mixing in the Y-sialon glass: Formation, properties and ballistic resistance", Journal of Non-Crystalline Solids, 2015 Publication	<1 %
36	oar.a-star.edu.sg Internet Source	<1 %
37	H. Y. Sastra, J. P. Siregar, S. M. Sapuan, M. M. Hamdan. " Tensile Properties of Fiber-Reinforced Epoxy Composites ", Polymer-Plastics Technology and Engineering, 2006 Publication	<1 %
38	Vanita Thakur, Anupinder Singh, R. Punia, Manpreet Kaur, Lakhwant Singh. "Effect of BaTiO3 on the structural and optical properties of lithium borate glasses", Ceramics International, 2015 Publication	<1 %
39	Vikas Attri, Vikas Attri. "Structural, Electrical and Optical Analysis of Barium Boro-Bismuthate Glass System: Opto-Electronic Devices", ECS Transactions, 2022 Publication	<1 %
40	research-information.bris.ac.uk Internet Source	<1 %
41	studentsrepo.um.edu.my Internet Source	<1 %
42	uokerbala.edu.iq Internet Source	

		<1 %
43	vdoc.pub Internet Source	<1 %
44	Ranjana Mehrotra, Heinz W. Siesler. "Application of Mid Infrared/Near Infrared Spectroscopy in Sugar Industry", Applied Spectroscopy Reviews, 2003 Publication	<1 %
45	Ton Duc Thang University Publication	<1 %
46	Submitted to University of Wolverhampton Student Paper	<1 %
47	Dash, Priyanka. "Dynamics of Space Charge Polarization and Electrical Conduction in Low Alkali Boroaluminosilicate Glasses.", Proquest, 2013. Publication	<1 %
48	Lakshminarayana, G., Kawa M. Kaky, S.O. Baki, Song Ye, A. Lira, I.V. Kityk, and M.A. Mahdi. "Concentration dependent structural, thermal, and optical features of Pr3+-doped multicomponent tellurite glasses", Journal of Alloys and Compounds, 2016. Publication	<1 %
49	Navneet Kaur Mattu, Kulvir Singh. "Structurally modified bioglasses synthesized using agro-food wastes and conventional sources for bone regeneration application", Ceramics International, 2023 Publication	<1 %
50	Zhiwei Luo, Gao Qu, Xingjun Chen, Xuefeng Liu, Anxian Lu. "Effects of nitrogen and lanthanum on the preparation and properties	<1 %

	of La–Ca–Si–Al–O–N oxynitride glasses", Journal of Non-Crystalline Solids, 2013 Publication	
51	www.politesi.polimi.it Internet Source	<1 %
52	www2.mdpi.com Internet Source	<1 %
53	ims.sxu.edu.cn Internet Source	<1 %
54	Submitted to Higher Education Commission Pakistan Student Paper	<1 %
55	Submitted to Jawaharlal Nehru Technological University Student Paper	<1 %
56	downloads.hindawi.com Internet Source	<1 %
57	dspace.ncl.res.in:8080 Internet Source	<1 %
58	dro.deakin.edu.au Internet Source	<1 %
59	etd.uwc.ac.za Internet Source	<1 %
60	H Doweidar. "Refractive index–structure correlations in silicate glasses", Journal of Non-Crystalline Solids, 2000 Publication	<1 %
61	Submitted to Texas Christian University Student Paper	<1 %
62	Yoshinari KATO, Hiroki YAMAZAKI, Yoshihiro KUBO, Satoshi YOSHIDA, Jun MATSUOKA, Tomoko AKAI. "Effect of B2O3 content on crack initiation under Vickers indentation	<1 %

	test", Journal of the Ceramic Society of Japan, 2010 Publication	
63	coek.info Internet Source	<1 %
64	qu.edu.iq Internet Source	<1 %
65	wiredspace.wits.ac.za Internet Source	<1 %
66	Fadgen, William. "Ferromagnetic and exchange bias studies in the diluted magnetic semiconductor (gallium,manganese) arsenide", Proquest, 20111004 Publication	<1 %
67	Fredriksson, A.. "An in situ ATR-FTIR study of the adsorption kinetics of xanthate on germanium", Colloids and Surfaces A: Physicochemical and Engineering Aspects, 20070720 Publication	<1 %
68	Hiroshi Yamashita, Hidetake Yoshino, Keishi Nagata, Hyuma Inoue, Takeshi Nakajin, Takashi Maekawa. "Nuclear magnetic resonance studies of alkaline earth phosphosilicate and aluminoborosilicate glasses", Journal of Non-Crystalline Solids, 2000 Publication	<1 %
69	Hu, Q.. "High-frequency FTIR absorption of SiO"2/Si nanowires", Chemical Physics Letters, 20030905 Publication	<1 %
70	Hugo Rodrigues Damasceno. "Solid-state NMR on the quadrupolar low-γ nucleus	<1 %

>sup<25>/sup
Publication

71	K.M Parida, Amarendra Samal. "Catalytic combustion of volatile organic compounds on Indian Ocean manganese nodules", Applied Catalysis A: General, 1999 Publication	<1 %
72	L. Aleksandrov, T. Komatsu, R. Iordanova, Y. Dimitriev. "Raman spectroscopic study of structure of WO3La2O3B2O3 glasses with no color and crystallization of LaBWO6", Optical Materials, 2011 Publication	<1 %
73	M.I. Sayyed, M.H.A. Mhareb, M. Kh. Hamad. "Physical, Mechanical, and ionizing radiation shielding properties of 10PbO–10Na2O-(80-x)B2O3-xBaO glasses", Optical Materials, 2024 Publication	<1 %
74	Mouad Garziad, Abdelmjid Saka, Hassane Moustabchir. "Structural Design and Simulation of the Collision Between a Pedestrian's Head and a Windshield of Vehicle", International Journal of Safety and Security Engineering, 2024 Publication	<1 %
75	Patwardhan, Pushkaraj R. "Understanding the product distribution from biomass fast pyrolysis", Proquest, 20111003 Publication	<1 %
76	Satoshi Yoshida, Yoshinari Nishikubo, Akiko Konno, Toru Sugawara, Yoshinari Miura, Jun Matsuoka. "Fracture- and Indentation-Induced Structural Changes of Sodium Borosilicate Glasses", International Journal of Applied Glass Science, 2012 Publication	<1 %

77	dspace.bits-pilani.ac.in:8080 Internet Source	<1 %
78	mdpi-res.com Internet Source	<1 %
79	savoirs.usherbrooke.ca Internet Source	<1 %
80	utpedia.utp.edu.my Internet Source	<1 %
81	vdocuments.site Internet Source	<1 %
82	A.M. Abdelghany, F.H. ElBatal, H.A. ElBatal, F.M. EzzElDin. "Optical and FTIR structural studies of CoO-doped sodium borate, sodium silicate and sodium phosphate glasses and effects of gamma irradiation-a comparative study", Journal of Molecular Structure, 2014 Publication	<1 %
83	Bin, Lee Ru. "Photo-Catalytic Degradation of Dye by Using Raw and Pre-treated Ilmenite", University of Malaya (Malaysia), 2023 Publication	<1 %
84	Dey, Sanj. "Elevated temperature lubricated wear of aluminum-silicon alloys", Proquest, 2012. Publication	<1 %
85	G. N. Greaves, S. Sen. "Inorganic glasses, glass-forming liquids and amorphizing solids", Advances in Physics, 2007 Publication	<1 %
86	H. Miyoshi, D. Chen, H. Masui, T. Yazawa, T. Akai. "Effect of calcium additive on structural changes under heat treatment in sodium borosilicate glasses", Journal of Non-Crystalline Solids, 2004	<1 %

Publication

87	Huirong Le, Kaibao Wang, Longyuan Li. "Geopolymers and Composites - Processing Technologies and Applications", CRC Press, 2025 Publication	<1 %
88	Itaru Enomoto, Yasuhiko Benino, Takumi Fujiwara, Takayuki Komatsu. "Synthesis of nanocrystals in KNb(Ge,Si)O5 glasses and chemical etching of nanocrystallized glass fibers", Journal of Solid State Chemistry, 2006 Publication	<1 %
89	J. T. Kloprogge, R. L. Frost. "Thermal decomposition of Ferrian chamosite: an infrared emission spectroscopic study", Contributions to Mineralogy and Petrology, 2000 Publication	<1 %
90	Kholood Alkhamis, Hawra A. Alghasham, Albandary Almahri, Hussain Alessa et al. "Iron borophosphate glasses: Merging optical transparency, structural integrity, and radiation shielding efficacy for sustainable uses", Arabian Journal of Chemistry, 2024 Publication	<1 %
91	Manish Jha, Amit K. Bhojani, Sachin Pathak, Vishakha Kaushik, Dheeraj K. Singh. "Raman spectroscopy: application to carbon-based nanomaterials", Elsevier BV, 2025 Publication	<1 %
92	Sandra Davison. "Conservation and Restoration of Glass", Butterworth-Heinemann, 2008 Publication	<1 %

93	Seyed Mojtaba Sadrameli. "Phase Change Materials for Energy Management and Efficiency", CRC Press, 2025 Publication	<1 %
94	Srikanta Moharana, Santosh Kumar Satpathy, Tuan Anh Nguyen, Ram K. Gupta, Parvej Ahmad Alvi. "Metal Oxide-based High-K Dielectrics - Fundamentals and Applications", CRC Press, 2025 Publication	<1 %
95	c.coek.info Internet Source	<1 %
96	gyan.iitg.ernet.in Internet Source	<1 %
97	open.uct.ac.za Internet Source	<1 %
98	pure.tue.nl Internet Source	<1 %
99	res.mdpi.com Internet Source	<1 %
100	scholar.sun.ac.za Internet Source	<1 %
101	scholarbank.nus.edu.sg Internet Source	<1 %
102	www.frontiersin.org Internet Source	<1 %
103	www.science.gov Internet Source	<1 %

Exclude quotes	On	Exclude matches	< 8 words
Exclude bibliography	On		

Santosh_Thesis_KUS2

GRADEMARK REPORT

FINAL GRADE

/100

GENERAL COMMENTS

PAGE 1

PAGE 2

PAGE 3

PAGE 4

PAGE 5

PAGE 6

PAGE 7

PAGE 8

PAGE 9

PAGE 10

PAGE 11

PAGE 12

PAGE 13

PAGE 14

PAGE 15

PAGE 16

PAGE 17

PAGE 18

PAGE 19

PAGE 20

PAGE 21

PAGE 22

PAGE 23

PAGE 24

PAGE 25

PAGE 26

PAGE 27

PAGE 28

PAGE 29

PAGE 30

PAGE 31

PAGE 32

PAGE 33

PAGE 34

PAGE 35

PAGE 36

PAGE 37

PAGE 38

PAGE 39

PAGE 40

PAGE 41

PAGE 42

PAGE 43

PAGE 44

PAGE 45

PAGE 46

PAGE 47

PAGE 48

PAGE 49

PAGE 50

PAGE 51

PAGE 52

PAGE 53

PAGE 54

PAGE 55

PAGE 56

PAGE 57

PAGE 58

PAGE 59

PAGE 60

PAGE 61

PAGE 62

PAGE 63

PAGE 64

PAGE 65

PAGE 66

PAGE 67

PAGE 68

PAGE 69

PAGE 70

PAGE 71

PAGE 72

PAGE 73

PAGE 74

PAGE 75

PAGE 76

PAGE 77

PAGE 78

PAGE 79

PAGE 80

PAGE 81

PAGE 82

PAGE 83

PAGE 84

PAGE 85

PAGE 86

PAGE 87

PAGE 88

PAGE 89

PAGE 90

PAGE 91

PAGE 92

PAGE 93

PAGE 94

PAGE 95

PAGE 96

PAGE 97

PAGE 98

PAGE 99

PAGE 100

PAGE 101

PAGE 102

PAGE 103

PAGE 104

PAGE 105

PAGE 106

PAGE 107

PAGE 108

PAGE 109

PAGE 110

PAGE 111

PAGE 112

PAGE 113

PAGE 114

PAGE 115

PAGE 116

PAGE 117

PAGE 118

PAGE 119

PAGE 120

PAGE 121

PAGE 122

PAGE 123

PAGE 124

PAGE 125

PAGE 126

PAGE 127

PAGE 128

PAGE 129

PAGE 130

PAGE 131

PAGE 132

PAGE 133

PAGE 134

PAGE 135